Published by :
http://www.ijert.org

International Journal of Engineering Research & Technology (IJERT)
ISSN: 2278-0181
Vol. 7 Issue 12, December-2018

Synopsis and Validation of Proposed Versatile Analytical Models for Advancing the Internal Stability Design of GMSE/GRS Geostructures

John Ngaya Mukabi
R&D/Design Dept.
Kensetsu Kaihatsu Consulting Engineers Ltd.
Nairobi, Kenya

Abstract **— The findings from current, on-going and past performance evaluation based on measurements of well instrumented GMSE (geosynthetics mechanically stabilized earth) and GRS (geosynthetic reinforced soil) geostructures provide definitively indisputable evidence that the conventional design methodologies for internal stability are excessively conservative, particularly with regard to the prediction of the prevalent reinforcement/tensile loads under in-service working conditions. This culminates in the exorbitant and unjustifiable use of public funds that would have otherwise been saved and invested in other development projects. As part of an absolutely necessary mitigation measure, this paper, within the R&D (research and development) framework of developing a pragmatic performance based value engineering design approach, presents an introduction of a set of proposed sophisticated analytical models that expound and explicate the influence factors proposed in the quasi-empirically developed K-Stiffness working stress method that takes into account, the structural contribution of global and local stiffness, wall facing rigidity, batter angle and cohesion (quality of reinforced backfill geomaterial properties), among other minor factors. The proposed analytical models are mainly validated and calibrated on the basis of measurements and performance data derived from a wide range of well instrumented GMSE-GRS geostructures as well as comparative analysis with reference to results obtained through the application of other analytical and/or numerical models. The versatility of the proposed analytical models is also discussed in this paper and fastidiously demonstrated in the other related papers to be published, which are cited herein. It is envisaged that the proposed TACH-MD analytical models are expedient for design and advancing R&D for GMSE-GRS retaining walls and bridge abutments.**

Keywords — GMSE-GRS, analytical models, internal stability, influence factors, K-Stiffness, TACH-MD, performance based, VE, value engineering, AASHTO, reinforced backfill geomaterial.

I. INTRODUCTION

A. Core of conservative approach and versatility of proposed analytical models

The conservative approach mainly emanates from the fact that the "true" mechanisms and interactive behavior between soil and geosynthetics reinforcement in GMSE-GRS geostructures including retaining walls and bridge abutments, has yet to be fully elucidated. As a consequence, practically all design guidance documents including those that are popularly adopted such as the AASHTO LRFD Bridge Design Specifications, 2012, AASHTO 2002, 2007; FHWA 2001; BS8006 1995; BS8006:2010, CFEM 2006; Geoguide 6 2002, NCMA 2009; PWRC 2000, among others, provide guidelines and specifications that are, by any standards, exceedingly conservative. On the other hand, the K-stiffness Method, which was empirically developed and calibrated based on post-construction structural performance of in-service GMSE-GRS Walls and first proposed by [1], quantitatively captures the influence of soil properties, reinforcement properties and structural wall facings on the magnitude of reinforcement loads under operational conditions, which leads to reasonable values for load and resistance factors.

This Study, within the R&D framework of performance based value engineering (PB-VE) design approach, takes advantage of the prodigious advances made in computer science, modelling and the research and methods of accurate measurements of in-service and full-scale experimental GMSE-GRS retaining walls and bridge abutments to propose TACH-MD universal analytical models that have been predominantly developed on the basis of these advances. The proposed analytical models provide considerable solutions to the aforementioned challenges and are versatile in application with appreciably high degree confidence levels. Case examples of the pragmatic applications of the proposed models for parametric investigations, characterization of various types of geomaterials, generation of performance-based value engineering designs, as well as development of special/particular specifications and construction QCA procedures, are also introduced in related publications ([2], [3], [4], [5], [6], [7] and [8]). It is also derived and concluded that appropriate application of the proposed analytical models can be useful in the enhanced prediction and precision of the maximum reinforcement/tensile loads, distribution characteristics, degree and well defined limitations of contribution factors, explicate characterization of the correlations between the influence factors and the principal design parameters including the GMSE-GRS wall height, H, geosynthetics base design length, L_{GD} and the vertical reinforcement spacing, S_v, development of appropriate VE designs for GMSE-GRS geostructures, seismic analysis, designation of appropriate serviceability state criteria and meticulous prediction of structural performance, among other diverse geotechnical engineering applications.

The intricate aspects and meticulous characterization of these influence factors are presented in a number of other related papers, soon to be published ([2] ~ [8]).

International Journal of Engineering Research & Technology (IJERT)
ISSN: 2278-0181
Vol. 7 Issue 12, December-2018

B. Limitations and incongruity of the conventional methods of GMSE-GRS design and internal stability analysis

Comprehensive literature review carried out on the State of the Art and State of the Practice international publications indicates that the design guidelines currently adopted by practically all transportation and infrastructure agencies clearly demonstrate the existence of certain limitations, which certainly require further R&D.

Some of these limitations, which have been outlined and/or discussed in detail in some of the State of the Art and State of the Practice international publications include: i) hitherto designs have been undertaken by manufacturers limiting them to proprietary philosophies, characteristics, approach and methodologies culminating in delayed development of generic design procedures; ii) due to the fact that soil-geosynthetics interactive mechanisms have not been well elucidated, design methods adopt extremely conservative procedures of determining the design parameters; iii) design methods consider simultaneous failure of both the reinforcing elements and reinforced backfill soils, which, from a scientific, soil mechanics and geotechnical engineering perspective, is highly unlikely; iv) design methods do NOT consider the effective structural and serviceability contribution of the wall facing; v) design methods do NOT consider the effective structural and serviceability contribution of incorporating geosynthetics reinforcement within the reinforced fill soil of GMSE-GRS geostructures; vi) compaction induced stresses are never considered in the design and analysis; vii) development of apparent cohesion and increased confining stress as a result of frictional, lateral and bearing restraint are never considered in the design and analysis; viii) no definitive models and/or appropriate procedures for determining optimal base design length and vertical reinforcement spacing exist; ix) lack of appropriate methods to determine required ultimate tensile and junction strengths of the reinforcing geosynthetics and/or elements, overtensioning and structural performance of GMSE-GRS RWs; x) practically all designs adopt a Rankine and/or Coulomb failure envelopes which do NOT consider the effective structural and serviceability contribution of incorporating geosynthetics reinforcement within the backfill soil of GMSE-GRS RWs; xi) no definitive models and/or appropriate procedures are incorporated for determining the required design reinforcement length for the base; xii) no definitive models and/or appropriate procedures are incorporated for determining the effects of wall facing inclination; and xiii) no scientific procedure and/or definitive models are incorporated for determining the required ultimate tensile and junction strengths of the reinforcing geosynthetics and/or elements, among other limitations.

C. Shortcomings of the limit equillibrium based methods

A number of disadvantages of limit equilibrium-based methods for internal stability design of geosynthetic reinforced soil walls which contribute to their poor prediction accuracy have been identified by various researchers and practicing engineers. For example, [9] identified the following shortcomings of limit equilibrium based methods: i) equilibrium is satisfied only for sliding mass modes of failure; ii) deformation is not considered; iii) in simplified methods, failure is allowed only on predefined surfaces; and iv) kinematics are not considered so that some failure mechanisms may not be possible.

As elucidated by [10] it is more appropriate to understand that this general approach results in simple models that do not satisfy a consistent mechanics framework but nevertheless result in conservative (safe) designs. Furthermore, the complex interactions that develop between a structural facing (a common feature of permanent walls) and the soil and reinforcement cannot be captured using simple wedge or slip surface models based only on force equilibrium. Reference [10] further state that; the persistence of limit equilibrium-based models for the internal stability design of geosynthetic reinforced design in current design codes is largely the result of lack of an alternative analytical approach. Nevertheless, the earliest attempts in North America to improve the prediction accuracy of geosynthetic reinforcement loads under operational conditions recognized that reinforcement loads were a function of displacement and hence the tensile stiffness of the reinforcement is a fundamental property for design [11]. An obvious contradictory paradox shortcoming of limit equilibrium methods that consider only the strength of the reinforcing elements is that predicted loads under operational conditions will be the same for steel and relatively extensible polymeric materials provided they have the same strength and number of layers in the wall.

D. Development of the K-Stiffness Method

Reference [12] investigated current North American methods for the prediction of reinforcement loads and concluded that the AASHTO Simplified Method [13] gave results similar to those of the other methods, yet had the advantage of being simpler to use and more broadly applicable. Consequently, [12] adopted the AASHTO Simplified Method as the baseline of comparison for predicted reinforcement loads using the new working stress method, the development of which they had undertaken based on long-term structural performance evaluation and case study analyses of well instrumented GMSE-GRS geostructures. Figure 1a clearly demonstrates the magnitude of deviation of the AASHTO Simplified Method from the actual measured reinforcement loads in geosynthetic walls built in the field.

E. Advancing the internal stability design approach within the Performanced-Based Value Engineering (PB-VE) design framework

Performance-Based Design (PBD) fundamentally entails that, deformation in ground, pavement materials and geo-structures along with the reciprocal structural deformation and stress states, be comprehensively analyzed by adopting appropriate sophisticated analytical methods, in order to achieve the predesignated structural and serviceability levels/requirements. The basic prerequisite of the PBD is that the acceptable level of the damage criteria be specified in engineering terms such as displacements, elastic limit stress state and ductility/ strain limit based on the function; as well dynamic loading and/ or seismic response of the structure.

One of the main objectives of developing the proposed analytical models is to contribute to the advancement of the design and analysis of the internal stability of GMSE-GRS

International Journal of Engineering Research & Technology (IJERT)
ISSN: 2278-0181
Vol. 7 Issue 12, December-2018

geostructures to transcend the conventional simplistic methods.

The TACH-MD models proposed in this paper have been developed for both Geosynthetics Mechanically Stabilized Earth (GMSE) and Geosynthetics Reinforced Soil (GRS) geostructures including retaining walls and bridge abutments.

II. OVERVIEW OF THE K-STIFFNESS METHOD WITHIN THE CONTEXT OF THE PROPOSED TACH-MD MODELS

A. Advantages of the K-Stiffness Method

GMSE-GRS walls are usually designed for working stress conditions simulating the post-construction state of in-service operations. [10] undertook comprehensive evaluation and concluded that one of the most effective working stress based methods is the empirically developed K-Stiffness Method. This method explicitly includes the influence of reinforcement stiffness and the structural facing amongst other contributions. Statistical analysis of the bias of measured to predicted load was used to demonstrate the improved accuracy of this new load design approach as demonstrated in Figure 1b.

Some of the inimitable aspects of this method include: i) an empirically based method developed for internal stability analysis from extensive case study analyses covering a wide range of GMSE-GRS wall types, facing rigidity, batter angles (facing inclinations), backfill soils and geosynthetic reinforcement types; ii) calibrated against more than fifty fully and partially well instrumented MSE-GRS walls constructed and constantly monitored over varying periods since 1986 to-date; iii) although other methods can be used to evaluate the potential for reinforcement rupture and pullout for the strength and extreme event limit states, only the K-Stiffness Method can be used to directly evaluate the potential for soil backfill failure and to design the wall internally for the service limit state; iv) discerns failure limit state of soil and reinforcement separately. Conventional methods including the AASHTO simplified method are based on active earth pressure theory or Coulomb wedge analysis and hence the soil and critical reinforcement layers are assumed to be simultaneously at incipient failure; v) explicitly includes the quantitative influence of reinforcement stiffness and structural facing contribution; vi) predicts reinforcement loads that are within a range of 10% of the post-construction operational actual measurements resulting in approximately 1/3 of the loads predicted using the models for the AASHTO simplified method. This culminates in more than 35% savings in the required reinforcement quantities.

Based on the foregoing attributes, the further refinement and advancement of the K-Stiffness method to satisfy the principal requirements of PB-VE designs certainly desirable.

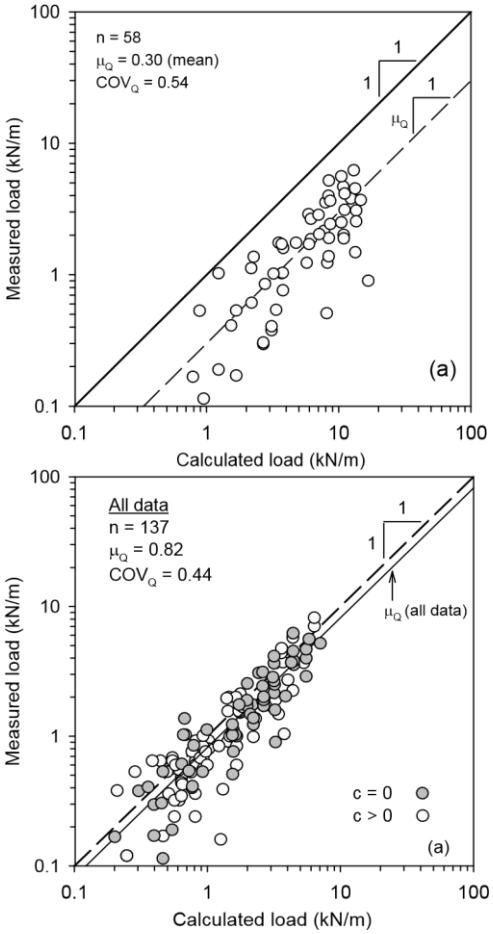

Fig. 1. Measured reinforcement load versus calculated load using the: a) AASHTO/FHWA Simplified Method; and b) K-stiffness Method (Bathurst et al., 2010).

B. Applicabilibity of the K-Stiffness Method and contribution of proposed TACH-MD analytical models

The K-Stiffness Method is empirically based with parameters that have been determined by calibration against a large database of carefully constructed, instrumented and monitored GMSE-GRS retaining wall structures. An important implication of this approach is that the method can only be used for structures with properties and boundary conditions that fall within the envelope of case study properties that were used to perform the calibration. For example, the wall heights in the database vary from $H = 3\ to\ H = 12.6\ m$. Hence, using the K-stiffness Method to design walls of greater height should be carried out with caution. Consequently, the models proposed in this and the related papers {[2] ~ [8]} enable probing of extrapolated application to greater heights (refer to Figures 3 and 4 as well as Figures 20 ~ 35 and the corresponding models defined in Equations 15 and 16 as well as Equations 33 ~ 50 presented in this paper). Also, the K-stiffness Method is applicable to walls built on typical competent foundations where the performance of the structures is not influenced by excessive settlements or failure of the foundation or wall toe. The TACH-MD models and methodology proposed in [7], [8] and [14] can be adopted to substantially mitigate this limitation.

International Journal of Engineering Research & Technology (IJERT)
ISSN: 2278-0181
Vol. 7 Issue 12, December-2018

On the other hand, most of the wall sections used to calibrate the K-Stiffness Method were constructed with a vertical face; with a limited number constructed with facing batter angles (ω) from: $\omega = 3°\ to\ \omega = 27$ (refer to Tables III and VI). As can be inferred, the analytical model proposed in Equation 36 and used in generating the characteristic curves graphically presented in Figures 25 and 26 can be effectively used in determining the appropriate limiting boundaries of the batter angle as a function of the shear strength of the reinforced backfill geomaterial. Furthermore, most of the walls were constructed with a hard structural facing. The TACH-MD analytical models proposed in [8], [15], and [16] can be adopted in modelling and determining the parameters required to achieve an optimal internal stability design mainly in consideration of the backfill quality and properties of the reinforcing elements for varying facing rigidity. A total of 58 data points were collected from 13 wall sections built with cohesionless soils and 79 data points from sections built with cohesive-frictional soils. The K-Stiffness Method in its most current form accounts for the positive contribution of soil cohesion to reduce geosynthetic reinforcement loads [17]. Indeed, it is extremely important to investigate the use of cohesive soils since purely frictional (granular) soils are hardly available and ignoring the cohesive component of available cohesive-frictional soils will lead to uneconomical structures. Equations 37 and 38 and the results depicted in Figures 27 and 28 demonstrate that the proposed analytical models can be useful to the design engineer in determining the appropriate value of the cohesion influence factor to adopt depending on the quality of the backfill soil.

Finally, it is perceived that the K-Stiffness Method was developed to compute reinforcement loads used for the internal stability design of reinforced soil retaining walls. At present the method applies only to internal rupture (over-stressing) and pullout failure modes (or limit states) and does not extend to the design of other structural components of the GMSE-GRS wall system. The method has also yet to cater for seismic loads. It is envisaged that the models proposed in this Study for seismic analysis, which are briefly introduced in this paper under Section VIII and discussed in detail in [6] can be applicable in alleviation. Refer to the models defined in Equations 30 ~ 32/51 ~ 53 as well as Figures 18 ~ 19/36 ~ 37.

Consequently, the K-Stiffness Method, as described by [1], is limited to the design of internal stability based on the following conditions: i) design internal stability for GMSE walls up to 12m in height; ii) GMSE Walls designed using this method should be constructed on sound foundations that are not supporting other structures and whose anticipated settlement is not greater than 150mm; iii) the method should be used for the design of walls with a maximum facing batter angle of: $\omega = 20°$; iv) at present the method applies only to internal rupture (over-stressing) and pullout failure modes (or limit states); v) other failure modes related to facing column stability, external stability and possible failure mechanisms that pass partially through the reinforced soil mass are beyond the scope of the method. For these failure modes current limit equilibrium-based models together with conventional factors of safety are available; and vi) the influence of additional loads due to earthquake has yet to be addressed within the K-stiffness Method framework. The necessity to review the foregoing limitations, as proposed in this Study, is therefore well appreciated.

C. Range of GMSE-GRS wall types and material properties studied within the K-Stiffness context

Key properties and parameters for each of the case histories referenced, including facing type, reinforcement geometry, reinforcement type, soil properties, and construction history, are discussed in detail by [18]. Wall reinforcement products included geotextiles and geogrids, different polymers (polypropylene (PP), high-density polyethylene (HDPE), and polyester (PET)), strip and continuous reinforcements, a range of tensile strengths from 12 to 200 kN/m, and reinforcement stiffness values from 90 to 7400 kN/m. Reinforcement vertical spacing varied from 0.3 to 1.6 m. Wall facing batter angles varied from 0° (vertical) to 27°, although most of the walls had facing batter angles of 5° or less. Wall heights varied from 4.0 to 12.6 m, with surcharge heights of up to 5.3 m of soil. Facing types included geosynthetic wrapped-face, welded wire, precast concrete panels, and modular concrete blocks (segmental retaining wall units). Estimated peak plane strain soil friction angles varied from 42 to 57°. Many of the conditions that are likely to be encountered in the field are included in the database of case histories described previously.

On the other hand, plane strain conditions are known to typically exist in reinforced soil walls. Peak plane strain friction angles for granular soils are larger than values from triaxial compression or direct shear testing and hence are less conservative for design. Furthermore, recent work indicates that the peak plane strain soil friction angle in calculations gives a better estimate of reinforcement loads, at least for geosynthetic walls ([19], [20], [21] and [22]). Peak friction angles reported in the source references from triaxial compression tests (ϕ_{tx}, in degrees) were corrected therefore to peak plane strain friction angles using the equation first proposed by [23]:

$$\phi_{PS} = 1.5\phi_{tx} - 17 \quad (1)$$

Based on interpretation of data presented by [24] and [25] for dense sands, values of ϕ_{PS} were calculated from peak direct shear friction angles, ϕ_{ds}, reported in the source references using the following relationship:

$$\phi_{PS} = tan^{-1}(1.2tan\phi_{ds}) \quad (2)$$

D. Accuracy of the K-Stiffness Method

The same database of measured reinforcement loads used to investigate the accuracy of the AASHTO Simplified Method was used by [17] to quantify the accuracy of the K-stiffness Method. The results are depicted in Figure 1a for the AASHTO Simplified Method and Figure 1b for the K-stiffness Method. Data for walls with cohesive-frictional and frictional soil backfills are included in these figures. The load bias statistics are almost the same for both data sets. The graphical plots in Figure 1b, for example, show that the data are distributed much closer to the 1:1 reference line for the K – stiffness Method than the corresponding data using the current AASHTO Simplified Method, which also exhibit a wide range of scatter (Figure 1b). The data show that the K-Stiffness Method does well in accurately capturing the measured load data for a range of wall heights and reasonable estimates of toe stiffness.

International Journal of Engineering Research & Technology (IJERT)
ISSN: 2278-0181
Vol. 7 Issue 12, December-2018

E. Universal model defining the maximum reinforcement load

The following key factors are known to influence the magnitude of the maximum reinforcement load, T_{max}: (i) height of the wall, H and any surcharge loads, q; (ii) global, S_{global} and local stiffness, S_{local} of the soil reinforcement; (iii) resistance to lateral movement caused by the stiffness of the facing, f_{stiff} and restraint at the wall toe, $t_{res.}$; (iv) face batter, $f_{batt.}$ (v) shear strength, s_u and stress–strain, $\sigma - \varepsilon$ behaviour which characterizes stiffness defined in terms of elastic modulus, E_0 of the soil; (vi) unit weight of the soil, γ_{rbf}; and (vii) vertical spacing of the reinforcement, S_v. These factors are introduced analytically in the generalized universal model delineated in Equation 3, which defines the maximum load per running unit length of wall in a reinforcement layer i:

$$T_{imax} = S_{vi}\sigma_h D_{tmax}\Phi \quad (3)$$

where S_{vi} is the tributary area (equivalent to the vertical spacing of the reinforcement in the vicinity of each layer when analyses are carried out per unit length of wall); σ_h is the lateral earth pressure acting over the tributary area; D_{tmax} is the load distribution factor that modifies the reinforcement load based on layer location; and Φ is the influence factor that is the product of factors that account for the effects of local and global reinforcement stiffness, facing stiffness, face batter and soil cohesion. On the other hand, the lateral pressure, σ_h is calculated as the average value over the height of the wall according to the conventional earth pressure theories, hence:

$$\sigma_h = \frac{1}{2}K\gamma_{rbf}(H + S) \quad (4)$$

where K is the lateral earth pressure coefficient, γ_{rbf} is the unit weight of the reinforced backfill, H is the height of the wall, and S is the equivalent height of uniform surcharge pressure q $(i.e., S = q/\gamma)$. The coefficient of lateral earth pressure K is calculated for a vertical GMSE Wall, i.e., batter angle equals to zero; $(\omega = 0)$ using the Jaky equation ([26]):

$$K = K_0 = K_{abv} = 1 - sin\left(\phi_{rbf}\right)_{PS} \quad (5a)$$

where $\left(\phi_{rbf}\right)_{PS}$ is the peak plane strain friction angle of the reinforced backfill soil. Note that, the use of $K = K_0$ in this proposed method does not imply that at-rest conditions exist within the reinforced backfill. K_0 is simply used as a familiar index parameter to characterize soil behaviour. For battered GMSE walls analyzed in this paper, a TACH-MD modified version of the simplified form of the Coulomb model, recommended by AASHTO, is adopted. This TACH-MD modified version, defined in Equation 5b, is compatible with the K-Stiffness Method.

$$K_{abh} = \frac{cos^2\left[\left(\phi_{rbf}\right)_{PS} + \omega\right]}{cos^2\omega\left(1 + \frac{sin\left(\phi_{rbf}\right)_{PS}}{cos\omega}\right)} \quad (5b)$$

Substituting for σ_h in Equation 3 yields:

$$T_{imax} = \frac{1}{2}K\gamma_{rbf}(H + S)S_{vi}D_{tmax}\Phi \quad (6)$$

Equation 6 contains an expression for reinforcement loads that is similar to the conventional expression used in current limit equilibrium methods of analysis but represents the average load applied to the reinforcement layers rather than a load that increases linearly as a function of the vertical overburden stress. The empirical reinforcement load distribution parameter D_{tmax} is used to distribute the load as a function of depth, accounting for the reinforcement properties, load redistribution among layers, and foundation conditions. It is expressed here as a function of normalized depth below the top of the wall $(z + S)/(H + S)$, including the effect of the soil surcharge S, and varies over the range $0 \le D_{tmax} \le 1$.

The modifier Φ is an empirically determined parameter that captures the effect the major wall components have on reinforcement load development. These parameters are used to improve the correlation between predicted and measured reinforcement loads at working stress conditions based on examination of a large number of case studies and wide range of database. For brevity, the influence factor Φ in Equation 6 is used to represent the product of five factors expressed in Equation 7 as follows:

$$\Phi = \Phi_g \times \Phi_{local} \times \Phi_{fs} \times \Phi_{fb} \times \Phi_c \quad (7)$$

Substituting for the modifier Φ in Equation 6 with the expanded factors from Equation 7 leads to an expanded universal model defined in Equation 8.

$$T_{imax} = \frac{1}{2}K\gamma_{rbf}(H + S)S_{vi}D_{tmax} \times \left[\Phi_g \times \Phi_{local} \times \Phi_{fs} \times \Phi_{fb} \times \Phi_c\right] \quad (8)$$

The terms Φ_g, Φ_{local}, Φ_{fs}, Φ_{fb} *and* Φ_c are influence factors that account for the effects of global and local reinforcement stiffness, facing stiffness, face batter and soil cohesion. This model captures all qualitative effects due to reinforcement stiffness, soil strength, facing stiffness and reinforcement arrangement expected by reinforced soil wall design engineers. The reinforcement load will increase as soil unit weight, γ_{rbf} and reinforcement spacing, S_v increases. Further details of the development of the original K-stiffness Method can be found in publications by [1] and [27]. The implementation of the original K-stiffness Method for cohesionless backfill soils can be found in [28] and [29]. Details of each influence factor and its computational approach are described next.

F. Influence of global stiffness factor

Parameter Φ_g is a global stiffness factor that accounts for the influence of the stiffness and passively, the spacing of the reinforcement layers over the entire wall height and is calculated as follows:

$$\Phi_g = \alpha\left[\frac{S_{global}}{P_a}\right]^{\beta} \quad (9)$$

Here, S_{global} is the global reinforcement stiffness whereas α and β are constant coefficients equal to 0.25 each. The non-dimensionality of the expression for global stiffness factor Φ_g is preserved by dividing the global reinforcement stiffness by $P_a = 101kPa$ (atmospheric pressure). The global reinforcement stiffness S_{global} accounts for the relative stiffness of the walls and is computed as follows:

$$S_{global} = \left[\frac{\sum J_i}{H}\right]^{a} \quad (10)$$

Here, $J_i = J_{2\%}$ is the tensile stiffness at the end of wall construction of an individual reinforcement layer expressed in units of force per unit length of wall: also note that: $T_{max} = J(\varepsilon, t) \times \varepsilon$. (see Figure 2).

The practical result of the formulation for global stiffness factor (Equation 10) is that as reinforcement stiffness increases and all other factors remain the same, reinforcement load (T_{max} in Equation 4-8) goes up. Parameter Φ_{local} is a local

International Journal of Engineering Research & Technology (IJERT)
ISSN: 2278-0181
Vol. 7 Issue 12, December-2018

stiffness factor that accounts for the relative stiffness of the reinforcement layer with respect to the average stiffness of all reinforcement layers and is expressed as:

$$\Phi_{local} = \left[\frac{S_{local}}{S_{global}}\right]^a \quad (11)$$

where "a" is a constant coefficient and S_{local} is the local reinforcement stiffness for reinforcement layer i calculated as:

$$S_{local} = \left[\frac{J}{S_v}\right]_i \quad (12)$$

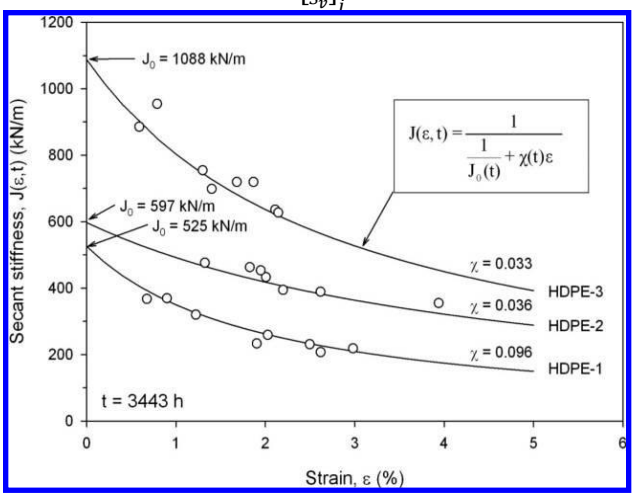

Fig. 2. Low-strain secant creep stiffness at t = 3443 h from laboratory constant-load (creep) tests (Allen & Bathurst, 2013).

G. Influence of facing batter

Parameter Φ_{fs} in the K-stiffness equation accounts for the influence of the facing batter and is computed as:

$$\Phi_{fb} = \left[\frac{K_{abh}}{K_{avh}}\right]^d \quad (13)$$

where, K_{abh} is the horizontal component of active earth pressure coefficient accounting for wall face batter, K_{avh} is the horizontal component of active earth pressure coefficient (assuming the wall is vertical), and "d" is a constant coefficient. The form of the equation shows that as the wall face batter angle $\omega \rightarrow 0$ (i.e. wall facing batter approaches the vertical) the facing batter factor $\Phi_{fb} \rightarrow 1$. The value of the coefficient term "d" is taken as 0.5.

H. Influence of wall facing stiffness

It is conventionally considered that: i) facings are incorporated to prevent a spill out of the backfill material; ii) earth pressure at the facing should be as low as possible; and, iii) facings should be flexible enough to accommodate deformation of supporting ground. However, on the contrary, [30] and [31] reported that: i) facing is a very essential structural component that actively confines the backfill and develops the necessary large tensile forces within the reinforcement; ii) earth pressure at facing should be high enough to provide sufficient confining pressure to the backfill; and, iii) the facing should be flexible enough to accommodate deformation of supporting ground during construction but should become rigid before service. Furthermore, [32] and [33] demonstrated that full-height or cast-in-place concrete facings increase the stability of geosynthetic reinforced retaining walls and introduced a coefficient α_{WF} that defines this correlation as expressed in the following Equation 14.

$$\alpha_{WF} = \left[\left(\frac{2}{K_a}\right)\left(\frac{\gamma_c}{\gamma}\right)\left(\frac{tan\phi_f - k_h}{1 - tan\phi_f tan\phi_w}\right)\right]\left(\frac{t}{h}\right) \quad (14)$$

The unit weight of the concrete, γ_c, is assumed to be 24kN/m^3. The wall and foundation friction angles, ϕ_w, and ϕ_f, respectively, are assumed to be 2/3 of the backfill angle of friction, ϕ. Based on these assumptions, it is clear from Equation 1 that the coefficient α_{WF} is dependent on only the t/h variable. Essentially, this equation indicates that as the wall thickness increases (i.e., α_{WF} increases), its capacity to carry active earth pressure increases.

In order to investigate the influence of wall facing stiffness on the structural performance of GMSE and GRS RW systems and verify and further authenticate the concept of wall facing contribution, [34] developed several models within the TACH-MD framework. In particular, two models of interest that are pertinent to the K-Stiffness Method, designed to quantitatively probe the structural wall facing contribution are: i) wall facing capacity – global stiffness model; and ii) universal wall facing stiffness - maximum tensile load – deflection model. The models are defined in Equations 15 and 16, whilst the characteristic curves depicting these correlations are graphically plotted in Figures 3 and 4 for descriptions i) and ii), respectively.

$$\delta_h = \frac{[0.7545H^2 + 0.3259H - 0.625]}{[1+\alpha_{WF}]} \ (mm) \quad (15)$$

$$J_{(CB)} = e^{-2.23ln[1.31\times10^{-3}(1+\alpha_{WF})\delta_{h(CB)}]} \ (kN/m) \quad (16)$$

where, δ_h is the lateral deflection, α_{WF} is the wall facing contribution factor, H is height of GMSE-GRS wall and $J_{(CB)}$ is the required reinforcement stiffness for modular concrete block (MCB).

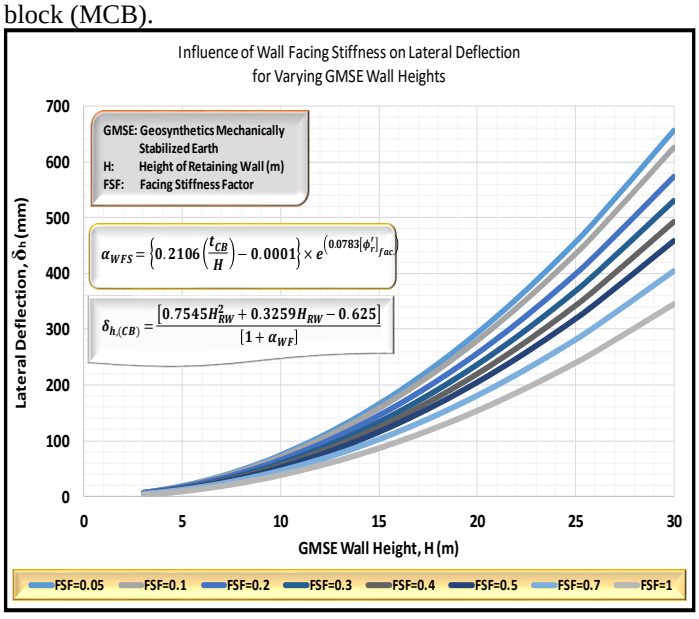

Fig. 3. Influence of wall facing stiffness on lateral displacement for varying wall heights (Mukabi et al., 2015).

The results in Figures 3 and 4 clearly indicate that: i) lateral deflection (straining deformation) decreases as wall facing stiffness increases implying that wall facing stiffness decreases deformation; and ii) wall facing stiffness increases the global stiffness of the retaining system (required tensile stiffness is reduced).

International Journal of Engineering Research & Technology (IJERT)
ISSN: 2278-0181
Vol. 7 Issue 12, December-2018

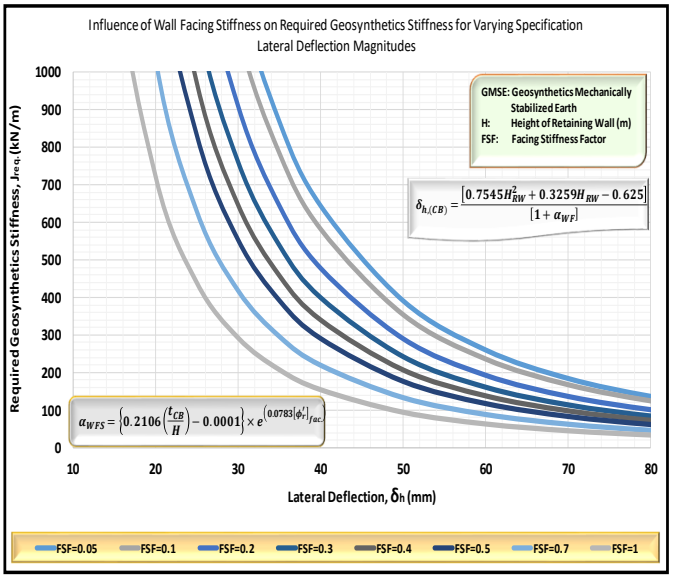

Fig. 4. Influence of wall facing stiffness on required tensile stiffness and lateral displacement (Mukabi et al., 2015).

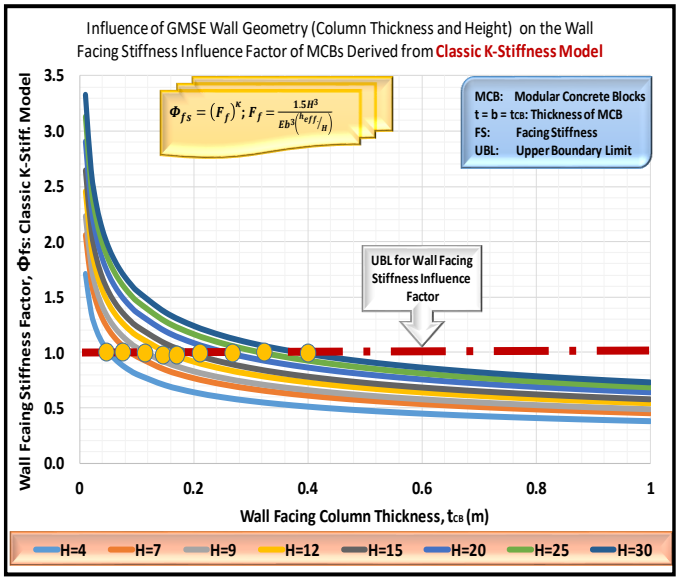

Fig. 5. Influence of GMSE-GRS Wall geometry (column thickness and height) on the wall facing stiffness influence factor derived from the classic K-Stiffness Model.

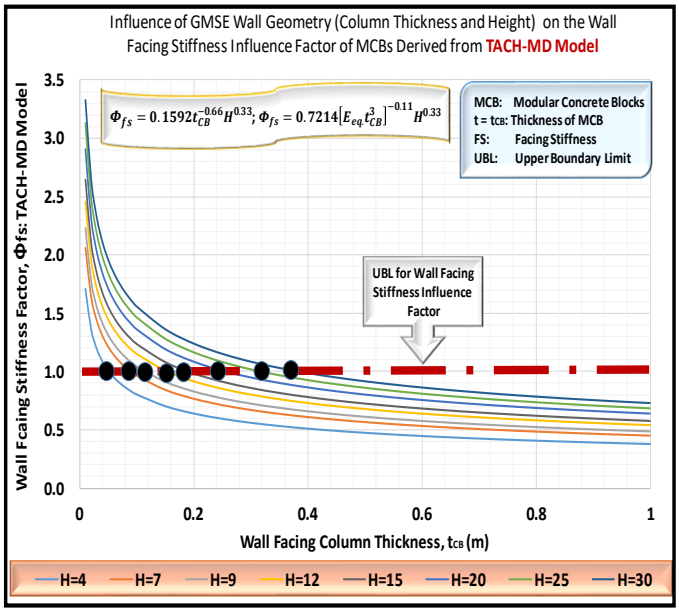

Fig. 6. Influence of GMSE-GRS Wall geometry (column thickness and height) on the wall facing stiffness influence factor derived from the classic K-Stiffness Model.

On the other hand, the K-Stiffness influence factor for facing stiffness (rigidity), Φ_{fs} is computed from the model defined in Equation 17 as:

$$\Phi_{fs} = \eta\left(F_f\right)^{\kappa} \tag{17}$$

In the latest version of the K-stiffness Method ([35]), the value of facing column stiffness parameter F_f is calculated as:

$$F_f = \frac{1.5H^3}{Eb^3\left({}^{h_{eff.}}/_{H}\right)} \tag{18}$$

Here, b = thickness of the facing column, H = height of the facing column (wall), and E = elastic modulus of the "equivalent elastic beam" representing the wall face. The two expressions used to compute the facing stiffness factor show that as the wall becomes higher (H) and less stiff (Eb^3), its rigidity becomes less and hence more load is carried by the reinforcement layers (i.e. Φ_{fs} is larger). A numerical investigation by [36] also predicted that reinforcement loads will increase in a propped panel wall as the stiffness of the facing decreases. This effect has been quantitatively demonstrated using measurements from a pair of full-scale reinforced soil walls tests reported by [37]. Based on back-analyses performed by [17] the coefficient terms η and κ were determined to be 0.69 and 0.11, respectively.

A comparison of characteristic curves depicting the influence of GMSE-GRS wall geometry (column thickness and height) on the wall facing stiffness influence factor derived from the classic K-Stiffness and the TACH-MD models can be inferred from Figures 5 and 6, respectively. It can be observed that the characteristic curves from these graphs superimpose perfectly. It is further derived from the same figures that: i) Φ_{fs} is highly dependent on the MCB facing thickness, t_{CB} and wall height; and ii) as can be anticipated, the contribution of the wall facing stiffness exhibits drastic reduction for thinner MCBs.

I. Influence of soil cohesion

The effect of soil cohesion is captured by the cohesion (influence) factor Φ_c computed as:

$$\Phi_c = 1 - \lambda\frac{c}{\gamma_{rbf}H} \tag{19}$$

where the cohesion coefficient $\lambda = 6.5$. Examination of this equation with $\lambda = 6.5$ reveals that the practical limit $0 \geq \Phi_c \geq 1$ requires $c/\gamma_{rbf}H \leq 0.153$. It is possible that a combination of a short wall height and high cohesive soil strength could lead to $\Phi_c = 0$. In practical terms this means that no reinforcement is required for internal stability. The TACH-MD models proposed in this paper do cater for this anomaly.

International Journal of Engineering Research & Technology (IJERT)
ISSN: 2278-0181
Vol. 7 Issue 12, December-2018

J. Characterization of load distribution

The load distribution factor, D_{tmax} that features in the principal universal Equations 3, 6 and 8 modifies the reinforcement load, T_{max} to effectively distribute and locate the appropriate critical failure surface. This parameter is computed as:

$$D_{tmax} = \frac{T_{max}}{T_{mxmx}} \quad (20)$$

where, T_{max} is the maximum reinforcement load in a particular layer i, whilst T_{mxmx} is the maximum reinforcement load for the entire system.

K. Locating appropriate critical failure surface

1) Comparison of the K-Stiffness and AASHTO simplified methods

The load distribution factor, D_{tmax} plotted against normalized height of wall in Figure 7 is essentially trapezoidal in shape as originally proposed by [1] or can be assumed to be bi-linear as plotted Figure 8.

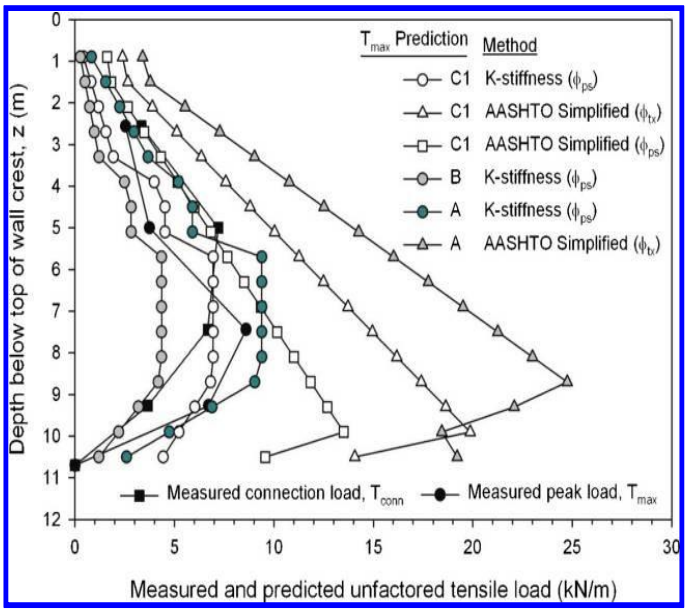

Fig. 7. Maximum load predictions (T_{max}) using AASHTO simplified method and *K*-stiffness method compared with measured load values at EOC (H = 10.7 m) deduced from measured strains. Notes: for class A predictions, $_{ps}$ = 41°, $_{tx}$ = 38°, and = 20.4 kN/m^3; for class B and C1 predictions, $_{ps}$ = 54°, $_{tx}$ = 47°, and = 22.0 kN/m^3 (Allen & Bathurst, 2013).

2) Influence of toe resistance Maximum Reinforcement Load (MRL) distribution

Figures 8a and 8b demonstrate that the distribution of the maximum reinforcement load is significantly influenced by the magnitude of the toe resistance.

It can be extrapolated from these figures that: i) the magnitude of the toe resistance not only impacts on the maximum reinforcement load distribution but also contributes immensely on the shape of the characteristic curves; ii) the characteristic curves are practically trapezoidal but tend towards linear as the toe resistance increases quantitatively (also refer to Figure 9); and iii) the AASHTO Simplified Method exceedingly overestimates the MRL.

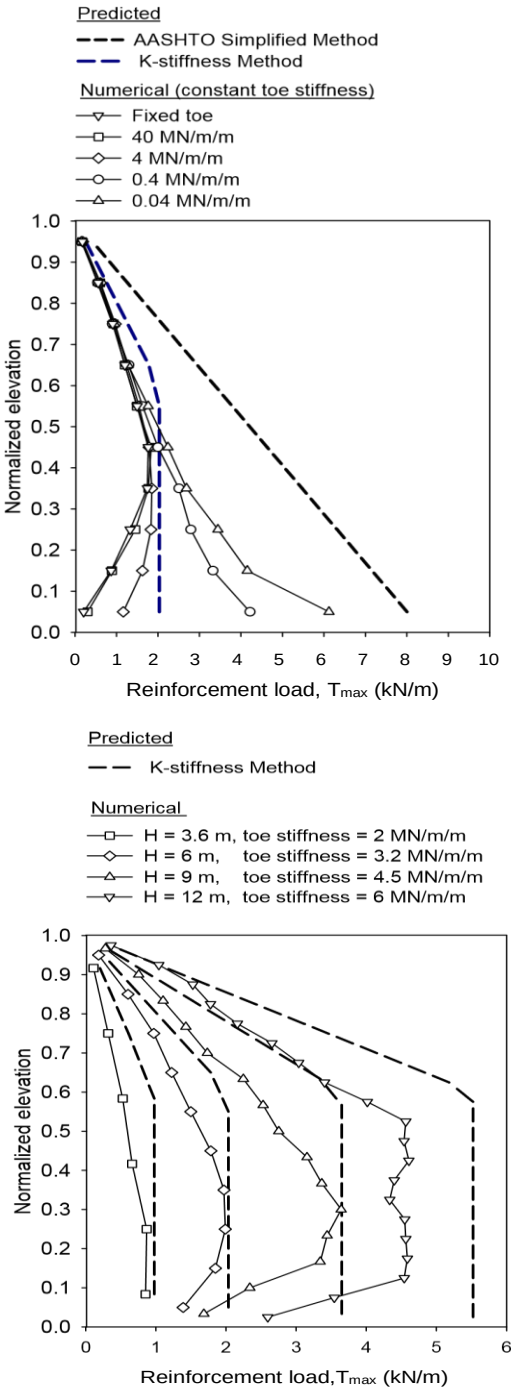

Fig. 8. Influence of (constant) toe stiffness on maximum reinforcement loads and comparison with predictions using: a) LHS - AASHTO Simplified Method and K-stiffness Method for wall with polyester (PET) reinforcement. (H = 6 m, S_v = 0.6 m, ω = 8 degrees). (after Huang et al. 2010); and b) RHS - K-stiffness Method for modular block wall with PET reinforcement. (S_v = 0.6 m, ω = 8 degrees) (Bathurst et al., 2010).

3) Effects of influence factors on maximum reinforcement load distribution

The findings from the R&D undertaken within the framework of the TACH-MD indicate that the influence factors have a significant effect on the distribution of the maximum reinforcement load magnitude and characteristics. An example is presented in Figure 9, which is a depiction of

International Journal of Engineering Research & Technology (IJERT)
ISSN: 2278-0181
Vol. 7 Issue 12, December-2018

the impact of the wall facing stiffness on the distribution of the MRL.

The characteristic curves plotted in Figure 9 were generated from model Equation 21. Also refer to Figures 13 ~ 16, presented in the subsequent Section III, which make a comparison of the measured and TACH-MD modelled results.

$$D_{tmax} = 0.858H^{0.234}\Phi_{fs}^{(0.6283H^{0.2792})} \quad (21)$$

$$\Phi_{fs} = exp\left\{(0.6283H^{0.2792})^{-1} ln\left[\frac{D_{tmax}}{0.858H^{0.234}}\right]\right\} \quad (22)$$

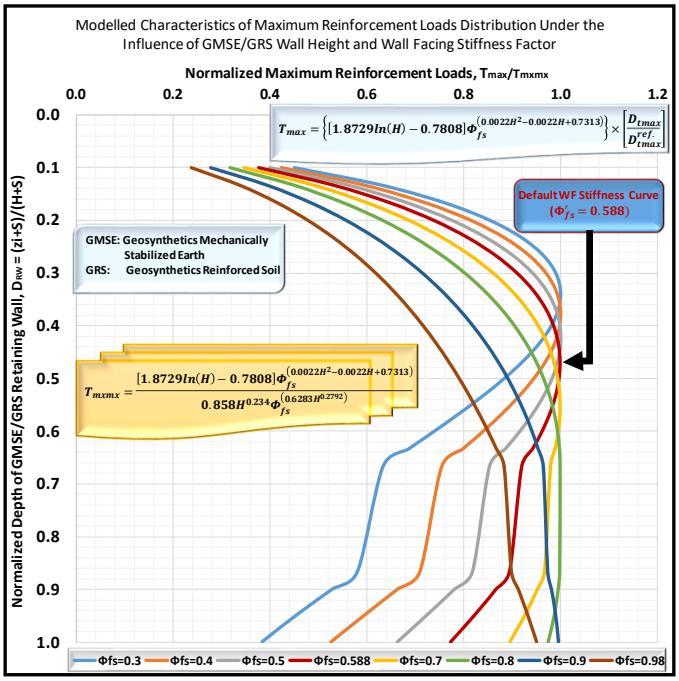

Fig. 9. Maximum reinforcement load distribution inluence factor, D_{tmax} plotted as a function of wall facing stiffness and GMSE wall height for vertical retaining walls wih cohesionless (granular) backfill $(c = 0)$.

The following observations can be made from Figure 9: i) the characteristic curves are essentially trapezoidal tending towards linear as the magitude of the wall facing influence factor increases, i.e., the wall facing stiffness is less or non-influencial; and ii) the MRL distribution and maximum values of the D_{tmax} vary with depth.

L. Calibration of the K-Stiffness classic models

The K-stiffness Method is an empirical-based working stress design method. The influence factors and coefficients which appear in the equations introduced above were determined by back-fitting to measured loads using conventional optimization schemes (see [33].) However, only reinforcement loads from walls that were judged to exhibit good performance were considered for the database used for calibration. Good performance was defined as: i) reinforcement strains are small (typically less than 3%); ii) creep strains and strain rates decrease with time (i.e. only primary creep occurs); iii) the wall backfill soil does not exhibit signs of failure (cracking, slumping, etc.); iv) for frictional soils, post-construction deformations, which are typically greatest at the wall top, are less than 30 mm within the first 10,000 h; and v) for cohesive-frictional soils, post-construction deformations are not greater than 300 mm or 3% of the height of the wall, whichever is less.

M. Internal soil failure limit state

An integral and unique feature of the K-stiffness Method is the introduction of an internal soil failure limit state. The calibration of the method has been based on the requirement that a contiguous failure mechanism must not develop through the reinforced soil zone. This has been achieved by limiting the maximum strain in the reinforcement to 3% based on load-time-strain performance of the reinforcing layers in geosynthetic reinforced soil walls. This is an important difference from the AASHTO Simplified Method and variants that assume that the soil and reinforcement reach failure simultaneously. The latter is a rare, if not impossible scenario for extensible geosynthetic reinforcement materials. Hence, designing to prevent soil failure is rational and safe, and at the same time ensures good performance as defined by the criteria identified earlier. In other words, designing to prevent failure of the soil in the reinforced soil zone deters the possiblility to reach a failure limit state for the reinforcement (rupture or over-stressing).

Pre-failure and failure mechanisms including the characteristics described in the foregoing paragraph are well elucidated based on the TACH-MD GMSE-GRS models developed for the K-Stiffness Method reported in this and the related papers in [2], [3], [4], [5], [6], [7] and [8]. The related papers, which further illuminate the versatility of the proposed models, focus on the following topics: i) correlation and characterization of principal influence factors [2] introduced in Section IV of this paper; ii) prediction and characterization of the maximum reinforcement load [3] introduced in Section V of this paper; iii) influence of quality of reinforced backfill geomaterials on the internal stability of GMSE-GRS retaining walls [4] introduced in Section VI of this paper; iv) influence of load carrying capacity and global stiffness of composite GMSE-GRS mass on internal stability [5] introduced in Section VII of this paper; v) seismic analysis in cogitation of the K-Stiffness influence factors [6] introduced in Section VIII of this paper; vi) application of TACH-MD GMSE-GRS analytical models in design and stability analysis [7] introduced in Section IX of this paper; and vii) establishment of appropriate serviceability criteria and prediction of structural performance [8] introduced in Section X of this paper.

III. VALIDATION OF THE TACH-MD MODELS DEVELOPED & PROPOSED WITHIN THE K-STIFFNESS FRAMEWORK

A. Lucidity of developing the TACH-MD GMSE-GRS models for the K-Stiffness Method

The lucidity of developing the TACH-MD K-Stiffness models is predominantly based on: i) the limitations elucidated in Section IA. of this paper; ii) the fact that the K-Stiffness Method is empirically developed hence the necessity to determine mechanistic models that correlate and diversely explicate the K-Stiffness influence factors accordingly; iii) necessity of defining and correlating the K-Stiffness influence factors to the wall geometry parameters in order to determine the magnitude/degree of influence; iv) necessity to define and correlate the K-Stiffness influence factors in terms of the interactive parameters that characterize the interaction

International Journal of Engineering Research & Technology (IJERT)
ISSN: 2278-0181
Vol. 7 Issue 12, December-2018

between the backfill geomaterial and the geosynthetics reinforcing elements within the reinforced zone; and v) importance of defining and correlating the K-Stiffness influence factors to the wall carrying capacity and stiffness parameters in order to better comprehend the characteristics and importance of taking the influence factors into account in design and stability analyses.

As a fundamental example of the lucidity of developing the TACH-MD GMSE-GRS K-Stiffness models, the TACH-MD model equivalents to Equations 1 and 2, which broaden the limits/range of application to make an approximate estimate of the plane strain soil friction angle, ϕ_{PS} based on triaxial, ϕ_{tx} or direct shear, ϕ_{ds} results, are proposed in Equations 23 and 24, respectively.

$$\phi_{PS} = 0.2563\phi_{tx}^{1.3878} \| \phi_{tx} \geq 34° \quad (23)$$

$$\phi_{PS} = 1.6197\phi_{ds}^{0.9019} \| \quad (24)$$

B. *Integral data adopted for development and calibration of TACH-MD GMSE-GRS models*

The integral data adopted for the development and calibration of the TACH-MD GMSE-GRS K-Stiffness models is mainly based on case histories as summarized and published by [36] for vertical/battered face geosynthetic-reinforced soil walls with cohesionless (granular) backfill and updated by [38] and [35] for vertical/battered face geosynthetic-reinforced soil walls with cohesive ($c - \phi$) soils as presented in Tables I, II and III.

TABLE I. CASE HISTORIES FOR VERTICAL FACE GEOSYNTHETICS-REINFORCED SOIL WALLS WITH COHESIONLESS (GRANULAR) BACKFILL (DATA FROM ALLEN ET AL., 2002A, 2003 AND MIYATA AND BATHURST, 2007A)

Wall case history and year built	Wall height (m)	Surcharge height (m)	Backfill: Soil unit weight (kN/m³)	Backfill: Peak friction angle[a] (ϕ) $_{tx}$ or $_{ds}$	Backfill: Peak friction angle[a] (ϕ) $_{ps}$	Facing type	Geosynthetic: Type	Geosynthetic: Designation	Geosynthetic: Index tensile strength[b] T_{ult} (kN/m)	Geosynthetic: J_{TS} (kN/m)	Geosynthetic: Measured T_{measd} (kN/m)	Performance[c]	Original reference
Tanque Verde Wall (GW5) 1984	4.7	0	19.6	53	53	Full-height propped concrete panel	Extruded drawn uniaxial HDPE	EGG-1	73	340	1.12	√	Bright et al. (1994)
Algonquin Wall (GW8) 1988	6.1	0	20.4	40	43	Incremental concrete panel		EGG-1	67.8	500	3.8	√	Christopher (1993)
Algonquin Wall (GW10) 1988	5.9	0	20.4	40	43	Wrapped-face	Nonwoven PET geotextile	NWGT-1	19.3	175	3.5	x	
RMC Wall (GW14) 1989	3	0	18	46	55	Full-height aluminium panel	Extruded drawn biaxial PP	EGG-2	12	90–95	0.38	√	Bathurst and Benjamin (1990)
RMC Wall (GW15) 1989	3	0	18	46	55	Incremental aluminium panel				87–93	0.53	√	Bathurst et al. (1993a)
Fredericton, New Brunswick Wall (GW18) 1990	6.1	0	20.4	42	45	Full-height propped concrete panel	Extruded drawn uniaxial HDPE	EGG-1	73	500	2.5	√	Knight and Valsangkar (1993)
FWRI Test Wall (GW21) 1988	4	0	16.7	31	31	Incremental plywood panel	Extruded drawn biaxial PP	EGG-3	18.2	130	6.01	x	FWRI (1988)
FWRI Test Wall (GW22) 1996	6	0	16.7	43	48	EPS block facing	Extruded drawn uniaxial HDPE	EGG-4	59.8	380	4.67	√	Tajiri et al. (1996)
FWRI Test Wall (GW23) 1996	6	0	16.7	43	48	Incremental concrete panel		EGG-4			4.14	√	
FWRI Test Wall (GW24) 1996	6	0	16.7	43	48	Full-height propped concrete panel		EGG-4			3.12	√	
FWRI Test Wall (GW25) 1996	6	0	16.7	43	48	Solid masonry block		EGG-4			1.9	√	
WSDOT SR-18 Wall GW26Cf 2005	10.7	0	22	–	54	Hollow masonry block with granular infill		EGG-5	62.5	350	5.61	√	Allen and Bathurst (2006)
								EGG-6	71.1	415			
								EGG-7	117	660			
WSDOT SR-18 Wall GW26D)	5.5	0	22	–	54			EGG-5	62.5	246	1.23	√	(unpublished data)

[a] $_{tx}$, $_{ds}$ are reported peak friction angle from triaxial compression tests and direct shear tests, respectively. $_{ps}$ is peak plane strain friction angle. [b]From in-isolation constant-rate-of-strain test carried out at 10% strain/minute. [c]Stiffness based on elapsed time to construct wall or 1000 h if this information not available. [d]Maximum reinforcement load in wall calculated using Equation 4; [e]¼ good performance, 3 ¼ poor performance. Performance criteria for walls with granular backfill as defined by Allen and Bathurst (2002b). [f]In previous related paper by Miyata and Bathurst (2007b) this wall was referred to as GW26.

TABLE II. CASE HISTORIES FOR VERTICAL FACE GEOSYNTHETICS-REINFORCED SOIL WALLS WITH COHESSIVE (C) SOILS (UPDATED DATA FROM MIYATA AND BATHURST, 2007A)

Wall case history and year built	Wall height (m)	Surcharge height[i] (m)	Backfill: Soil unit weight (kN/m³)	Backfill: Fines content (%)	Backfill: Peak friction angle[a] (°) $_{tx}$ or $_{ds}$ (c ≥ 0)	Backfill: Peak friction angle[a] (°) $_{ps}$ (c - 0)	Backfill: Cohesion c (kPa)	Facing type	Geosynthetic: Type	Geosynthetic: Designation	Geosynthetic: Index tensile strength[b] T_{ult} (kN/m)	Geosynthetic: J_{TS} (kN/m)	Geosynthetic: Measured T_{measd} (kN/m)	Performance[c]	Original reference
FWRI Wall (GW27) 1987	4	0.5	17	25	29	31	29	4.9	Gabion basket with soil-cement	Extruded drawn uniaxial HDPE	EGG-8	71.4	400	8.2	√	PWRI et al. (1988)
FWRI Wall (GW28) 1987									Gabion basket with crushed stone					10.6	x	
FWRI Wall (GW29) 1987									Wrapped-face with sand bags					11.2	x	
FWRI Wall (GW30) 1985	8	0	18.5	25	31	34	31	10	Hollow masonry concrete block with granular infill		EGG-4	59.8	380	1.98	√	Ochiai and Fukuda (1996)
Fugoshima Wall (GW31) 1984	4	0.4	15.2	20–40	39	46	44	4.9	Geotextile wrapped-face		EGG-8	71.4	400	0.92	√	Yamanouchi et al. (1986a)
Yamaguchi Wall (GW32) Sections I, & J 1985	6	0.4	17.4	6	36	44	40	12.8	Incremental concrete panel		EGG-8	71.4	400	I.: 0.48 R: 0.76	√	Yamanouchi et al. (1986b)
TRC (GW33i) 1998	5.4	0	18.8	91	24	29	28	1.4	Hollow masonry concrete block with granular infill	Extruded drawn uniaxial HDPE	EGG-9	35.0[k]	100[k]	2	√	Farrag et al. (2004)
TRC (GW33i) 1998											EGG-10	70.0[f]	250[k]	4.53	√	
TRC (GW33ii) 1998											EGG-11	114	500	5.75	√	
(GW40) 1992	4	0	16.2	8	38	42	40	2	Incremental concrete panel	Extruded drawn biaxial PP	EGG-15	32	170	0.83	√	PWRC (1995)
(GW42) 1992	4	0	15.5	8	38	42	40	2	Plywood panel	Extruded drawn uniaxial HDPE	EGG-4	59.8	400	2.72	√	

[a]See Appendix A for method to calculate peak plane strain friction angles. [b]From in-isolation constant-rate-of-strain test carried out at 10% strain/minute. [c]Stiffness based on elapsed time to construct wall or 1000 h if this information not available. [d]Maximum reinforcement load in wall calculated using Equation 4. [e]Soil–cement properties estimated from data reported by Yu et al. (1997). The equivalent elastic modulus of the soil-cement mixture in the wall was reduced to reflect the shorter curing time in the field. [f]From manufacturers' literature. [g]Estimated from tensile test carried out at 2.5% strain/minute reported by Farrag et al. (2004) and increased to value expected for a test carried out at 10% strain/min based on data presented by Miyata and Bathurst (2007b) for EGG-4. [h]No creep data available – value estimated from EGG-10 and EGG-11 stiffness values and correlation between ultimate strength and secant stiffness value for uniaxial HDPE geogrids reported by Walters et al. (2002). [i]¼ good performance, 3 ¼ poor performance. Criteria for good performance of walls with c– soils given in Section 4. [j]Broken back surcharge profile – maximum equivalent uniform surcharge calculated using the total weight of the maximum surcharge over the reinforced soil zone divided by the width of the reinforced soil zone.

TABLE III. CASE HISTORIES FOR WALLS WITH A FACING BATTER ($\omega > 0$) UPDATED FROM ALLEN ET AL. (2002A, 2003)

Wall case history and year built	Wall height (m)	Surcharge height[i] (m)	Backfill: Soil unit weight (kN/m³)	Backfill: Fines content (%)	Backfill: Friction angle[a] (°) $_{tx}$ or $_{ds}$ (c ≥ 0)	Backfill: Friction angle[a] (°) $_{ps}$ (c - 0)	Backfill: Cohesion c (kPa)	Facing: Type	Facing: Batter angle (°)	Geosynthetic: Type	Geosynthetic: Designation	Geosynthetic: Index tensile strength T_{ult} (kN/m)	Geosynthetic: J_{TS} (kN/m)	Geosynthetic: Measured T_{measd}	Performance[c]	Original reference
Jobs, Norway, Section J and I (GW7) 1987	4.8	J: 1.75 N: 1.3	17	3	41	46	46	0	Welded wire	27	Extruded drawn uniaxial HDPE	EGG-12	53.1	350	J: 1.47 N: 2.21	√	Fannin and Hermann (1990)
Algonquin, ON (GW9) 1988	6.1	1.2	20.4	0	40	43	43	0	Hollow modular masonry block with granular infill	3	Woven PET geogrid	WGG-1	39.2	200	1.26	√	Bathurst et al. (1993b)
Reinforcement, USA (GW16) 1989	12.6	2.7	21.1	0	45	54	54	0	Wrapped face	3	Woven PP geotextile	WGT-1	31	120	5.2	√	Allen et al. (1992)
												WGT-2	62	190		√	
												WGT-3	92	340			
											Woven PET geotextile	WGT-4	186	1000		√	
Tenza, Italy (GW20hp) 1998	4	2.4	21.1	10	47	57	55	8	Welded wire	5	Extruded drawn uniaxial HDPE	EGG-13	56.3	300	0.87	√	Carrubba et al. (1999)
Tenza, Italy (GW20hpp) 1998	4	2.5	21.1	10	47	57	55	8	Welded wire	5	Extruded drawn PP	EGG-14	20.9	90–100	0.55	√	
FWRI Wall (GW35) 1990	4.5	0.5	18.6	25	24	27	24	4.9	Gabion basket with sand bags	6	Extruded drawn uniaxial HDPE	EGG-4	59.8[f]	380	1.6	x	Nakane et al. (1990); Onodera et al. (2004)
FWRI Wall (GW36) 1917	6.3	0	16	0	41	46	45	2	Sand bags (not wrapped)	11		EGG-4	59.8[f]	380	1.56	√	Miki et al. (1992)
Fugoshima Wall (GW37) 1984	6	0.9	14.7	6	45	52	51	2.5	Wrapped-face with sand bags	17		EGG-8	71.4[f]	400	1	√	Yamanouchi et al. (1986a)
Fugoro Wall (GW38) 1987	7.5	0.5	16.1	75	25	27	25	12	Wrapped-face with sand bags	11		EGG-8	71.4[f]	400	2	√	Itoh et al. -1988
Takama Wall (GW39) 1989	8.7	0.9	19.7	6	44	53	51	17	Wrapped-face with sand bags	27		EGG-4	59.8[f]	380	0.68	√	Abe et al. -1989
(GW41) 1992	4	0	16	8	38	42	40	2	Sand bags	11.3		EGG-4	59.8[f]	400	1.68	√	PWRC (1995)

[a]See Appendix A for method to calculate peak plane strain friction angles. [b]Broken back surcharge profile – maximum equivalent uniform surcharge calculated using the total weight of the maximum surcharge over the reinforced soil zone divided by the width of the reinforced soil zone. [c]Stiffness based on elapsed time to construct wall or 1000 h if this information was not available. [d]End-of-construction values corresponding to S < 1 m. [e]¼ good performance, 3 ¼ poor performance of walls with c– soils based on criteria given in Section 4. [f]HDPE geogrid tensile strength adjusted to values estimated from 10% strain/minute tests;. [g]Date of construction not reported by Miki et al. (1992) assumed as 1991.

C. Comparison of measured vs. TACH-MD modelled data

Comparison of measured data vs. results that were modelled based on TACH-MD GMSE-GRS models developed for the K-Stiffness Method is the most fundamental approach adopted in the validation and calibration of the proposed models. In so doing, four principal parameters including: i) the secant stiffness at the end of construction (EOC) or @ 2% strain, J_{EOC} *or* $J_{@\varepsilon=2\%}$; ii) maximum reinforcement (tensile) load, T_{max} ; iii) global maximum reinforcement load, T_{mxmx} ; and iv) the maximum load distribution influence factor, D_{tmax} are adopted. Under this topic, comparison of small strain secant stiffness, $J_{@\varepsilon\leq 0.1\%}$ characteristics with progressive straining, $\varepsilon \leq 0.1\%$; and seismic analysis using plots of characteristic curves generated from TACH-MD GMSE-GRS models is also made employing measured data and modelled results.

Note that the TACH-MD GMSE-GRS models for the K-Stiffness Method were specifically developed for the modular concrete blocks (MCBs), which are the most commonly used for wall facings in Kenya.

Tables IV ~ VI present a summarized tabulation of measured and modelled results derived from the case history data shown in Tables I ~ III. On the other hand, graphical comparisons are depicted in Figures 10 ~ 28. In general, it can be derived that, the characteristic curves generated from the TACH-MD GMSE-GRS models in cogitation of similar conditions exhibit an appreciably good agreement with the measured data and are compatible (harmonious) with the classic K-Stiffness models.

1) Tabulated summary of measured vs. modelled results

The measured and TACH-MD modelled results are summarized in Tables IV ~ VI.

TABLE IV. COMPARISON OF MODEL COMPUTED RESULTS AND MEASURED DATA FROM TABLE I

Case histories for vertical face geosynthetic-reinforced soil walls with cohesionless (granular) backfill

Wall case history and year built	Wall height (m)	Surcharge height (m)	Backfill: Soil unit weight (kN/m³)	Backfill: Peak friction angle (°)	Facing type	Geosynthetic: Type	Geosynthetic: Designation	Geosynthetic: Index tensile strength (kN/m)	$J_{@\varepsilon\leq 2\%}$ (kN/m): Measured	$J_{@\varepsilon\leq 2\%}$ (kN/m): Computed	T_{mxmx} (kN/m): Measured	T_{mxmx} (kN/m): Computed	T_{max} (kN/m): Measured	T_{max} (kN/m): Computed	Equation 7 $f_{(H,Dtmax)}$	Equation 8 $f_{(H,\phi)}$	Original reference
Jaspe Bede Wall (W5) 1984	4.7	0	19.6	53	53	Full-height propped concrete panel	Extruded drawn uniaxial HDPE	EGG-1	73	340	439	1.12	1.58	0.90	1.29	1.09	Bright et al. (1994)
Ajaxpain Wall (2W9) 1988	6.1	0	20.4	40	43	Incremental concrete panel		EGG-1	67.8	500	413	3.8	2.08	3.04	1.62	2.24	Christopher (1993)
Ajaxpain Wall (2W10) 1988	5.9	0	20.4	40	43	Wrapped-face	Nonwoven PET geotextile	NWGT-1	19.3	175	148	3.5	2.02	2.80	1.57	2.16	
MC Wall (2W14) 1989	3	0	18	46	55	Full-height aluminium panel	Extruded drawn biaxial PP	EGG-2	12	90~95	101	0.38	1.03	0.30	0.86	0.79	Barbarat and Benjamin (1990)
MC Wall (2W15) 1989	3	0	18	46	55	Incremental aluminium panel				87~93		0.53	1.05	0.42	0.86	0.79	Barbarat et al. (1993a)
Fredericton, New Brunswick Wall (2W18) 1990	6.1	0	20.4	42	45	Full-height propped concrete panel	Extruded drawn uniaxial HDPE	EGG-1	73	500	439	2.5	2.05	2.00	1.62	2.10	Knight and Valsangkar (1993)
WRI Test Wall (2W21) 1988	4	0	16.7	31	31	Incremental plywood panel	Extruded drawn biaxial PP	EGG-3	18.2	130	142	6.01	1.48	4.81	1.11	1.83	PWRI (1988)
WRI Test Wall (2W22) 1996	6	0	16.7	43	48	EPS block facing	Extruded drawn uniaxial HDPE	EGG-4	59.8	380	373	4.67	2.07	3.74	1.60	1.99	Tajiri et al. (1996)
WRI Test Wall (2W23) 1996	6	0	16.7	43	48	Incremental concrete panel		EGG-4				4.14	2.06	3.31	1.60		
WRI Test Wall (2W24) 1996	6	0	16.7	43	48	Full-height propped concrete panel		EGG-4				3.12	2.04	2.50	1.60		
WRI Test Wall (2W25) 1996	6	0	16.7	43	48	Solid masonry block		EGG-4	23			1.9	1.99	1.52	1.60	1.99	Model Compatible Facing
VSDOT SR-8 Wall (2W26C) 1995	10.7	0	22	–	54	Hollow masonry block with granular infill		EGG-5	62.5	350	387	5.61	3.44	4.49	2.69	2.07	Allen and Bathurst (2006)
								EGG-6	71.1	415	429						
								EGG-7	117	660	644						
VSDOT SR-8 Wall (2W26D)	5.5	0	22	–	54			EGG-5	62.5	246	387	1.23	1.82	0.98	1.48	1.26	(unpublished data)

TABLE V. COMPARISON OF MODEL COMPUTED RESULTS AND MEASURED DATA FROM TABLE II

Case histories for vertical face geosynthetic-reinforced soil walls with cohesive backfill soil

Wall case history and year built	Wall height (m)	Surcharge height (m)	Backfill: Soil unit weight (kN/m³)	Backfill: Fines content (%)	Backfill: Peak friction angle (°)	Backfill: Cohesion c (kPa)	Facing type	Geosynthetic: Type	Geosynthetic: Designation	Geosynthetic: Index tensile strength (kN/m)	$J_{@\varepsilon\leq 2\%}$ (kN/m): Measured	$J_{@\varepsilon\leq 2\%}$ (kN/m): Computed	T_{mxmx} (kN/m): Measured	T_{mxmx} (kN/m): Computed	Equation 7 $f_{(H,Dtmax)}$	Equation 8 $f_{(H,\phi)}$	Original reference
WRI Wall (2W27) 1987	4	0.5	17	25	29	4.9	Gabion basket with soil-cement	Extruded drawn uniaxial HDPE	EGG-8	71.4	400	431	8.2	1.11	1.83		PWRI et al. (1988)
WRI Wall (2W28) 1987							Gabion basket with crushed stone						10.6				
WRI Wall (2W29) 1987							Wrapped-face with sand bags						11.2				
WRI Wall (2W30) 1995	8	0	18.5	25	31	10	Hollow masonry concrete block with granular infill		EGG-4	59.8	380	373	1.98	2.07	3.64		Ochiai and Fukuda (1996) MQC
Yugoshima Wall (2W31) 1984	4	0.4	15.2	20~40	39	4.9	Geotextile wrapped-face		EGG-8	71.4	400	431	0.92	1.11	1.13		Yamanouchi et al. (1986a)
Yamaguchi Wall (2W32) Sections I, & J 1985	6	0.4	17.4	6	36	12.8	Incremental concrete panel		EGG-8	71.4	400	431	I.: 0.48 R: 0.76	1.60	1.93		Yamanouchi et al. (1986b)
TRC (2W33i) 1998	5.4	0	18.8	91	24	1.4	Hollow masonry concrete block with granular infill	Extruded drawn uniaxial HDPE	EGG-9	35	100	241	2	1.45	2.81		Farrag et al. (2004) MQC
TRC (2W33ii) 1998									EGG-10	70	250	424	4.53				
TRC (2W33iii) 1998									EGG-11	114	500	631	5.75				
(2W40) 1992	4	0	16.2	8	38	2	Incremental concrete panel	Extruded drawn biaxial PP	EGG-15	32	170	224	0.83	1.11	1.29		PWRC (1995)
(2W42) 1992	4	0	15.5	8	38	2	Plywood panel	Extruded drawn uniaxial HDPE	EGG-4	59.8	400	373	2.72	1.11	1.29		

TABLE VI. COMPARISON OF MODEL COMPUTED RESULTS AND MEASURED DATA FROM TABLE III

Case Histories for Walls with a Facing Batter (α > 0)

Wall case history and year built	Wall height (m)	Surcharge height (m)	Backfill: Soil unit weight (kN/m³)	Backfill: Fines content (%)	Backfill: Friction angle (°)	Backfill: Cohesion c (kPa)	Facing: Type	Facing: Batter angle (°)	Geosynthetic: Type	Geosynthetic: Designation	Geosynthetic: Index tensile strength (kN/m)	$J_{@\varepsilon\leq 2\%}$ (kN/m): Measured	$J_{@\varepsilon\leq 2\%}$ (kN/m): Computed	T_{mxmx} (kN/m): Measured	T_{mxmx} (kN/m): Computed	Equation 7 $f_{(H,Dtmax)}$	Equation 8 $f_{(H,\phi)}$	Original reference
Oslo, Norway, Section J (2W7) 1987	4.8	J: 1.75 N: 1.3	17	3	41	0	Welded wire	27	Extruded drawn uniaxial HDPE	EGG-12	53.1	350	339	J: 1.47 N: 2.21	1.31	1.40	Fannin and Hermann (1990)
Ajaxpain, SA (2W9) 1988	6.1	1.2	20.4	0	40	3	Hollow modular masonry block with granular infill	3	Woven PET geogrid	WGG-1	39.2	200	264	1.26	1.62	2.03	Barbarat et al. (1993b) MQC
Jaiser Avenue, SA (2W16) 1989	12.6	2.7	21.1	0	45	0	Wrapped face	3	Woven PP geotextile	WGT-1	31	120	218	5.2	3.12	2.08	Allen et al. (1992)
										WGT-2	62	190	384				
										WGT-3	92	340	530				
									Woven PET geotextile	WGT-4	186	1000	940				
Ajaxpain, Italy (2W28(Bp)) 1988	4	2.4	21.1	10	47	8	Welded wire	5	Extruded drawn uniaxial HDPE	EGG-13	56.3	300	355	0.87	1.11	0.79	Carnuba et al. (1999)
Ajaxpain, Italy (2W28(Bp)) 1998	4	2.5	21.1	10	47	8	Welded wire	5	Extruded drawn PP	EGG-14	20.9	90~100	158	0.55	1.11	0.79	
WRI Wall (2W35) 1990	4.5	0.5	18.6	25	24	4.9	Gabion basket with sand bags	6	Extruded drawn uniaxial HDPE	EGG-4	59.8	380	373	1.6	1.24	2.41	Nakane et al. (1990); Tatsuoka et al. (2004)
WRI Wall (2W36) 1991	6.3	0	16	0	41	2	Sand bags (not wrapped)	11		EGG-4	59.8	380	373	1.56	1.67	1.89	Miki et al. (1992)
Yugoshima Trial (2W37) 1984	6	0.9	14.7	6	45	2.5	Wrapped-face with sand bags	17		EGG-8	71.4	400	431	1	1.60	1.47	Yamanouchi et al. (1986a)
Nagano Trial (2W38) 1987	7.5	0.5	16.1	75	25	12	Wrapped-face with sand bags	11		EGG-8	71.4	400	431	2	1.95	4.37	Itoh et al. (1988)
Hitama Trial (2W39) 1989	8.7	0.9	19.7	6	44	17	Wrapped-face with sand bags	27		EGG-4	59.8	380	373	0.68	2.23	1.96	Abe et al. (1989)
(2W41) 1992	4	0	16	8	38	2	Sand bags	11.3		EGG-4	59.8	400	373	1.68	1.11	1.29	PWRC (1995)

2) Measured vs. modelled results for EOC secant modulus

Figure 10 makes a comparison between measured data and results derived on the basis of TACH-MD GMSE-GRS models developed for the secant stiffness determined at the end of construction, J_{EOC} as defined in Equation 25.

$$J_{EOC} = 13.323 T_{ult.}^{0.8145} \quad (25)$$

International Journal of Engineering Research & Technology (IJERT)
ISSN: 2278-0181
Vol. 7 Issue 12, December-2018

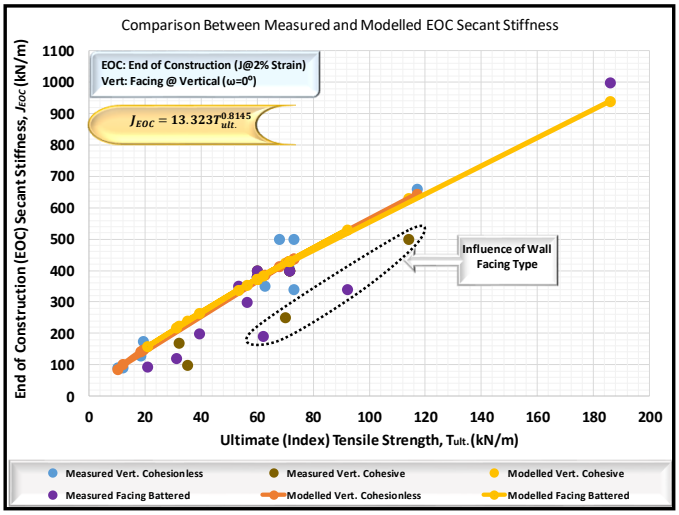

Fig. 10. Comparison between measured and TACH-MD modelled Secant Stiffness @ EOC (End of Construction), J_{EOC}.

It can be noted, from the results provided in Figure 10, that: i) the measured and modelled results show a close agreement; and ii) the wall facing type has an appreciable influence on secant stiffness measured at the end of construction.

3) Measured vs. modelled results for Tmax

The comparison between measured data and TACH-MD results modelled from Equation 26 for the maximum reinforcement load, T_{max}, is presented in Figure 11.

Note that $D_{tmax}^{ref.} = 0.8$ in all model equations that contain the term $D_{tmax}/D_{tmax}^{ref.}$ in this paper.

$$T_{max} = \left\{[1.8729ln(H) - 0.7808]\Phi_{fs}^{(0.0022H^2-0.0022H+0.7313)}\right\} \times \left[\frac{D_{tmax}}{D_{tmax}^{ref.}}\right] \quad (26)$$

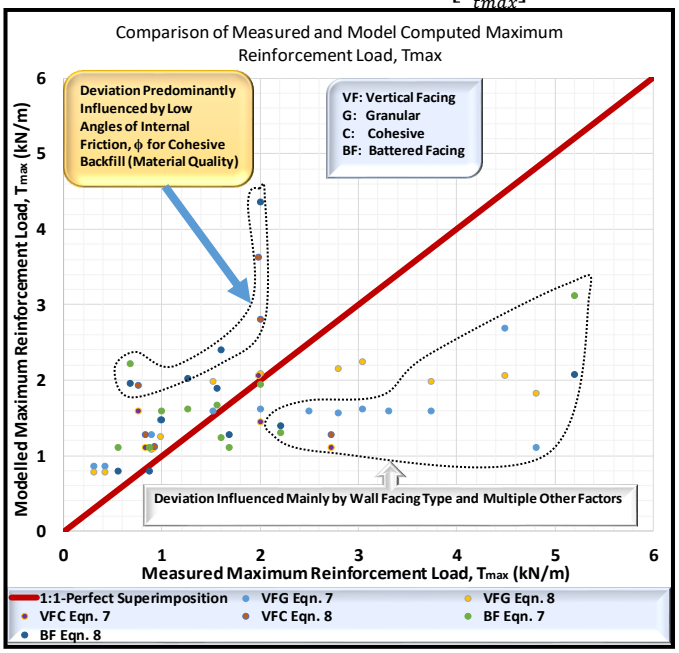

Fig. 11. Comparison between measured and TACH-MD modelled maximum reinforcement (tensile) load, T_{max}.

It can be noted, that: i) for higher reinforced backfill shear strength (angle of internal friction/shearing resistance) under similar structural conditions, the measured and modelled results show an appreciably good agreement; and ii) in conformity with the universal Equation 8, the GMSE-GRS wall height, surcharge, wall facing type, backfill geomaterial quality, vertical reinforcement spacing and facing batter angle have a significant influence on maximum reinforcement load.

4) Measured vs. modelled results for Tmxmx

Figure 12 provides a comparison between measured data and TACH-MD modelled results based on Equation 27 for the global maximum reinforcement load, T_{mxmx} . Similar observations can be made to those irradiated for the T_{max} in the preceding sub-Section 3.

$$T_{mxmx} = \frac{T_{max}}{2.3476H^{-0.851}T_{max}^{(-0.00014H^2+0.0013H+0.9538)}} \quad (27)$$

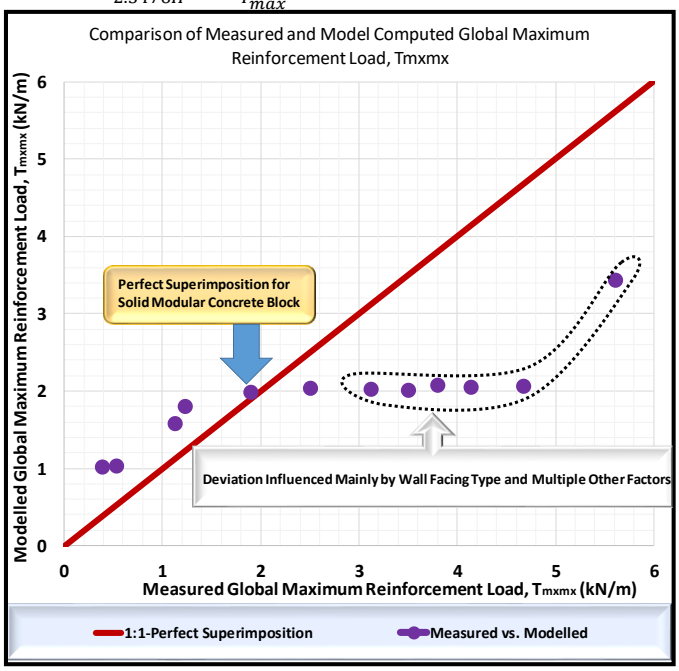

Fig. 12. Comparison between measured and TACH-MD modelled global maximum reinforcement (tensile) load, T_{mxmx}.

5) Measured vs. modelled results for Dtmax

The comparison between measured data and TACH-MD results modelled from Equation 28 for the distribution of maximum reinforcement load, T_{max} is graphically presented in Figures 13 ~ 16 principally as a function of the wall facing stiffness influence factor for varying reinforced backfill geomaterial type and batter angles.

$$D_{tmax} = T_{max}/T_{mxmx}\ 0.858H^{0.234}\Phi_{fs}^{(0.6283H^{0.2792})} \quad (28)$$

It can be noted, that: i) when compared under similar structural conditions, the measured and modelled results exhibit an appreciably good agreement; ii) the wall facing stiffness has significant influence on the magnitude and characteristics of the maximum reinforcement load distribution; iii) the nature/quality of backfill geomaterial and batter angle also do have appreciable influence on the MRL distribution.

International Journal of Engineering Research & Technology (IJERT)
ISSN: 2278-0181
Vol. 7 Issue 12, December-2018

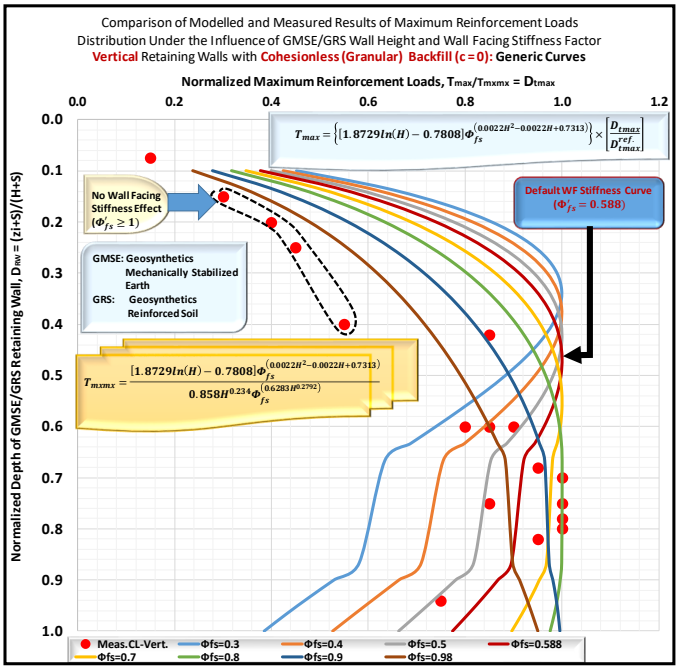

Fig. 13. Comparison between measured and TACH-MD modelled results for maximum reinforcement (tensile) load distribution inluence factor, D_{tmax} plotted as a function of wall facing stiffness and GMSE wall height for vertical retaining walls wih cohesionless (granular) backfill $(c = 0)$.

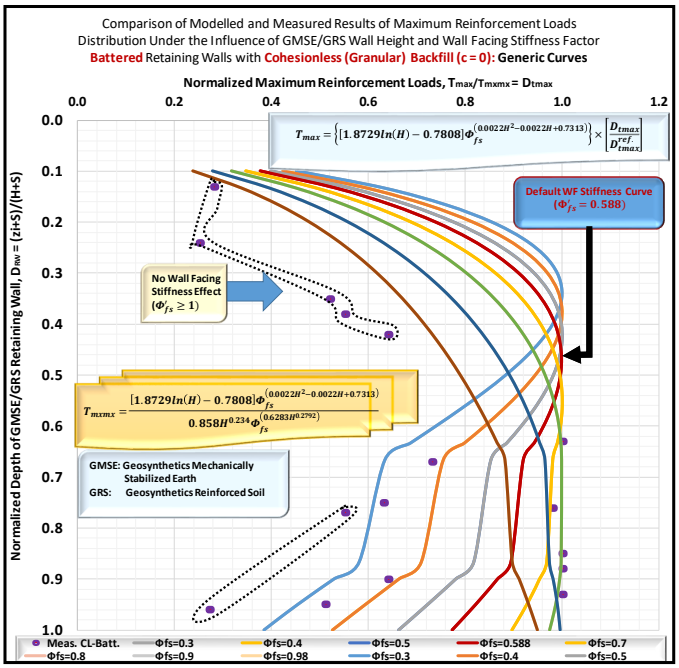

Fig. 14. Comparison between measured and TACH-MD modelled results for maximum reinforcement (tensile) load distribution inluence factor, D_{tmax} plotted as a function of wall facing stiffness and GMSE wall height for battered retaining walls wih cohesionless (granular) backfill $(c = 0)$.

Figure 16, which compares measured and TACH-MD modelled results for cohesive backfill with battered facing shows that most data points plot along the maximum distribution value of $D_{tmax} = 1$.

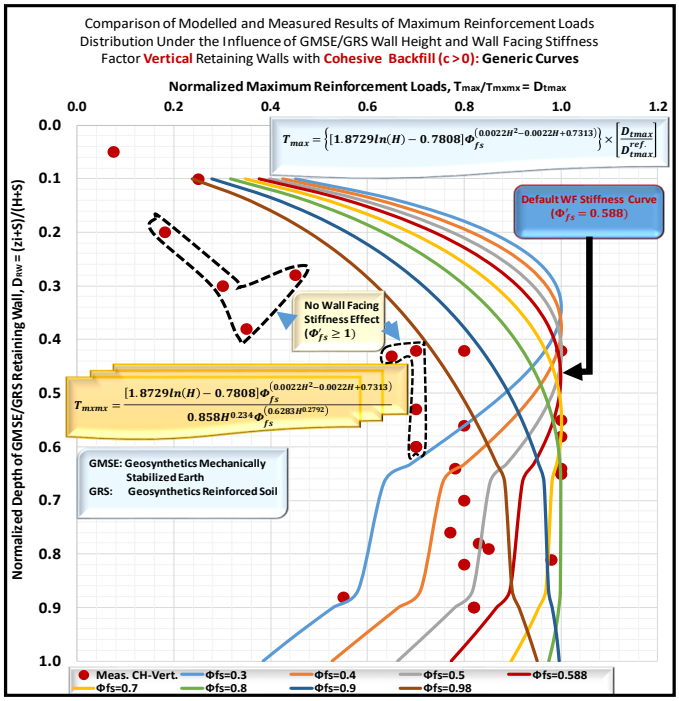

Fig. 15. Comparison between measured and TACH-MD modelled results for maximum reinforcement (tensile) load distribution inluence factor, D_{tmax} plotted as a function of wall facing stiffness and GMSE wall height for vertical retaining walls wih cohesive backfill $(c > 0)$.

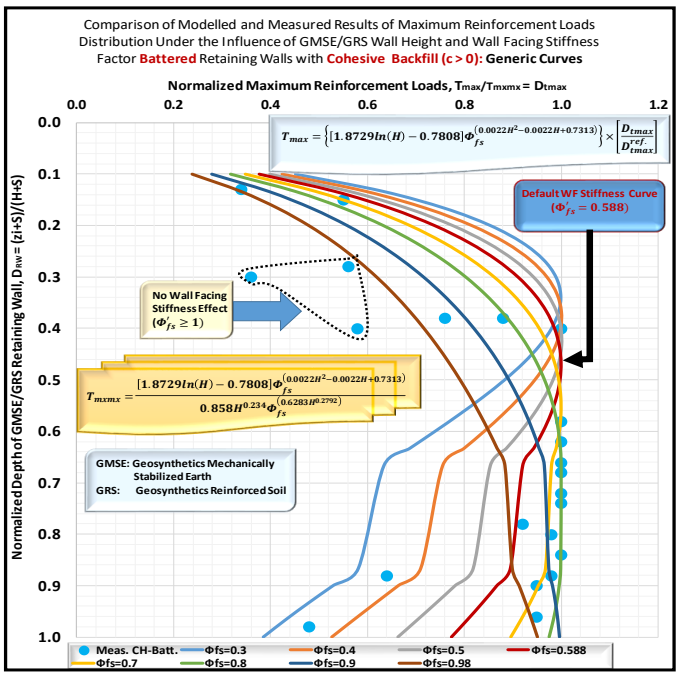

Fig. 16. Comparison between measured and TACH-MD modelled results for maximum reinforcement (tensile) load distribution inluence factor, D_{tmax} plotted as a function of wall facing stiffness and GMSE wall height for battered retaining walls wih cohesive backfill $(c > 0)$.

6) Measured vs. modelled results for secant modulus decay characteristics with progressive straining

The comparison between measured and TACH-MD modelled results for the decay characteristics for reinforcement secant stiffness with progressive straining are graphically plotted in Figure 17 for three different initial stiffness values. The modelled curves are generated from Equation 29.

International Journal of Engineering Research & Technology (IJERT)
ISSN: 2278-0181
Vol. 7 Issue 12, December-2018

$$J_{@\geq 0.1\%} = -63.38exp(0.000994J_0)ln(\varepsilon) + 571.29ln(J_0) - 3326.3 \quad (29)$$

The results in Figure 27 show a perfect superimposition for the lowest initial stiffness value of $J_0 = 600\,kN/m$ and a very good agreement for the other two curves; $J_0 \cong 800$ and $J_0 \cong 1000\ kN/m$. The fact that the reinforcement secant stiffness decays rapidly within the initial zone of small strains $\varepsilon \leq 0.6\%$ tending to a residual state as the straining progresses, in all cases, can also be derived from this figure.

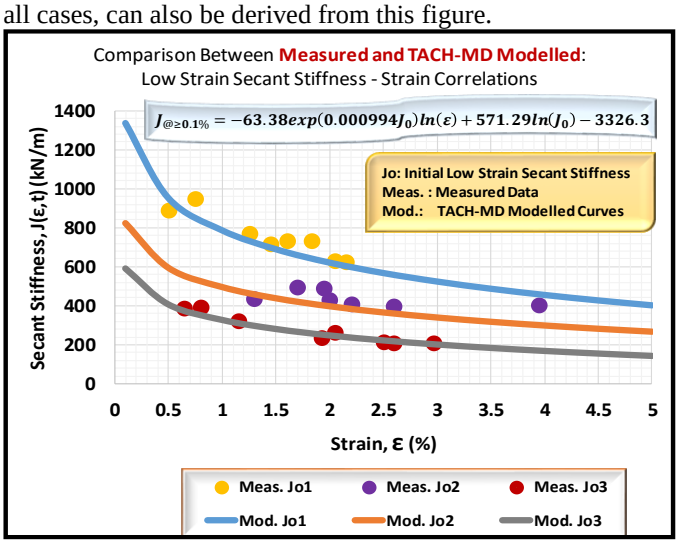

Fig. 17. Comparison between measured and TACH-MD modelled low strain secant stiffness – strain correlations.

7) Comparison of modelled results for seismic analysis

Development of TACH-MD models that can be adopted for seismic analysis for the K-Stiffness Method has also been undertaken. Some of the models that have been developed and proposed are introduced in this paper in the generalized Equations 30 ~ 32 and in the particular Equations 51 ~ 53. Equation 30 is adopted in investigating the influence of reinforced backfill shear strength and the GMSE-GRS wall geometry on the seismic force coefficient, K. The results reported by [39] and [40] are compared, in Figure 18, to those generated from the TACH-MD model Equation 30. The harmonic agreement is seen to be exemplary.

$$K = -0.000259\phi'^{2.2765}_{rbf}\left({}^{t}/_{H}\right) - 0.49ln\left(\phi'_{rbf}\right) + 2.1392 \quad (30)$$

The influence of seismic acceleration and backfill properties on coefficient of seismic pressure can be computed from the TACH-MD model Equations 31 and 32. The results, showing a perfect agreement, are compared in Figure 19 to those reported by [41] and [40].

$$K_a = -0.3818exp(2.2693a)ln\left(\phi'_{rbf}\right) + 1.5686exp(2.3868a) \quad (31)$$

$$K_a = -(7.8333a^3 - 0.4a^2 + 0.7017a + 0.393))ln\left(\phi'_{rbf}\right) + 29.467a^3 - 1.055a^2 + 3.2938a + 1.6045 \quad (32)$$

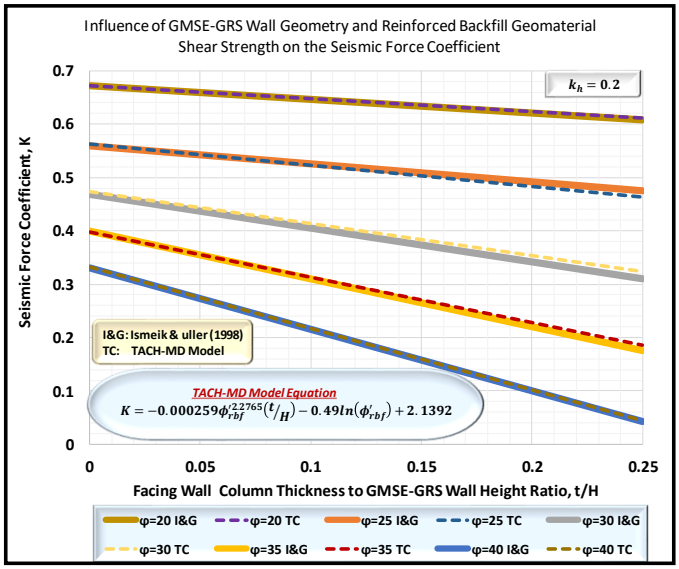

Fig. 18. Influence of quality of reinforced backfill geomaterial defined in terms of shear strength (angle of internal friction) and GMSE-GRS wall geometry on the seismic force coefficient: TACH-MD modelled results, Koseki et al., 2006 (also refer to Figure 36).

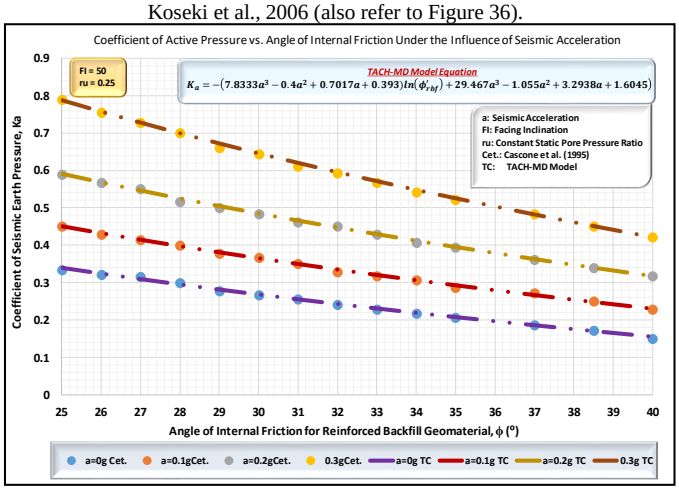

Fig. 19. Influence of quality of reinforced backfill geomaterial defined in terms of shear strength (angle of internal friction) and seismic acceleration on the coefficient of seismic earth pressure: TACH-MD modelled results, Koseki et al., 2006 (also refer to Figure 37).

D. Comparison of classic K-Stiffness and TACH-MD models

The other approach that was adopted in validating the TACH-MD GMSE-GRS models developed for the K-Stiffness Method is based on the comparative analysis of the TACH-MD and classic K-Stiffness principal models, the results of which are presented in Figures 20 ~ 29.

1) Comparison of global stiffness influence factor models

Figure 20 depicts the characteristic curves generated from back-calculation using the classic K-Stiffness model Equation 8, whilst Figures 21 and 22 show the graphical plots based on the TACH-MD models for the global influence factor generated from Equations 33 and 34, respectively.

$$\Phi_g = 0.2859H^{0.1411}T_{max}^{-[0.0922exp(-0.033H)]} \times \left[\frac{D_{tmax}}{D_{tmax}^{ref.}}\right] \quad (33)$$

$$\Phi_g = 0.3143exp(0.0136H)\Phi_{fs}^{[-0.0601exp(0.0232H)]} \times \left[\frac{D_{tmax}}{D_{tmax}^{ref.}}\right] \quad (34)$$

International Journal of Engineering Research & Technology (IJERT)
ISSN: 2278-0181
Vol. 7 Issue 12, December-2018

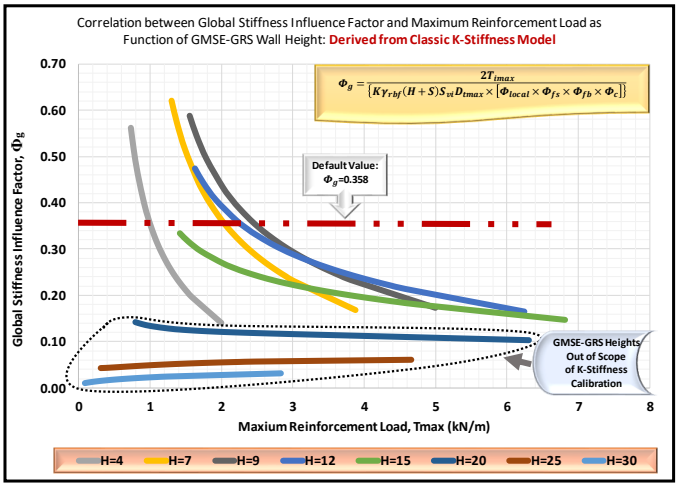

Fig. 20. Characteristic curves generated from the classic K-Stiffness model back-calculation for the global stiffness influence factor.

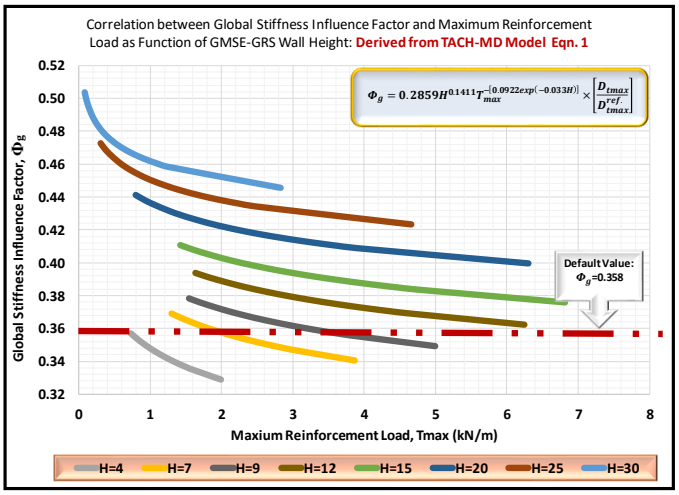

Fig. 21. Derivation of th global stiffness influence factor based on TACH-MD model equation 1 (Equation 33), which correlates Φ_g with angle of internal friction of reinforced backfill geomaterialand GMSE wall height.

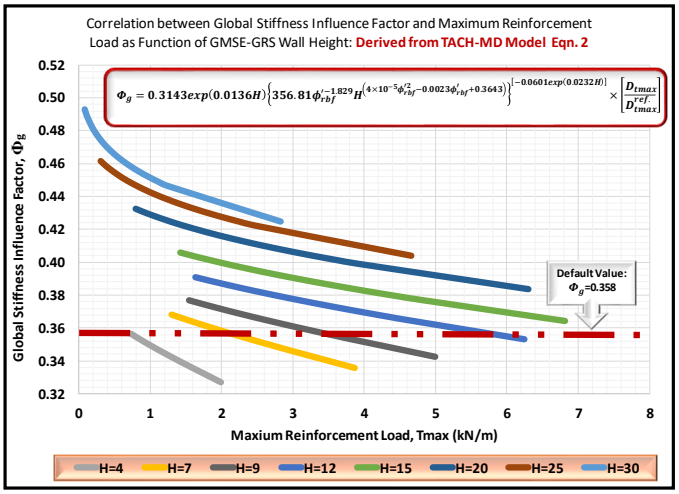

Fig. 22. Comparison of results computed using TACH-MD model equation 2 (Equation 34).

The direct comparison of the results generated from the classic K-Stiffness and TACH-MD models for the global stiffness influence factor is made in Figure 23. Note that the scale has been blown up for clearer perception.

It can be observed that the data from both models is in appreciably close proximity with all the data points plotting within 10% difference (deviation). The slight difference is mainly attributed to the fact that default values were used for the influence factors in the classic K-Stiffness model, whilst the data generated from the TACH-MD model adopted reciprocal variables. This fact can be ascertained by comparing the data point in yellow that is within the closest proximity to the default value whereby the deviation from the line of perfect superimposition is only 1.13%. Note that this data point was generated using default values for both models.

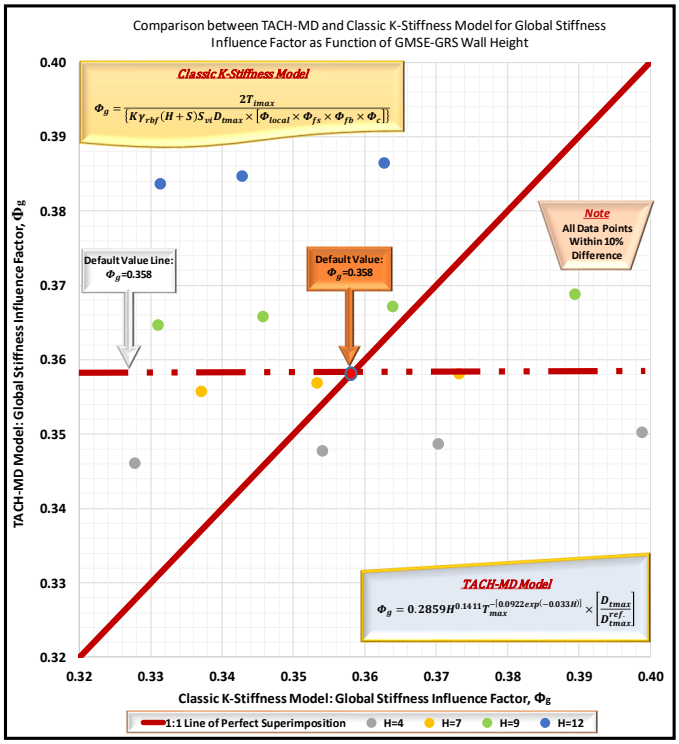

Fig. 23. Comparison between K-Stiffness and TACH-MD models for the global stiffness influence factor.

2) Comparison of wall facing stiffness influence factor models

Comparison of the wall facing stiffness influence factor generated from the two models is made in Figure 24. The wall facing stiffness factor is plotted as a function of the wall facing column thickness in both cases. The characteristic curves for the K-Stiffness models are generated from Equations 17 and 18, whilst the ones for the TACH-MD model are generated from Equations 35. Note that the wall facing considered is the modular concrete block (CB) commonly used in Kenya.

$$\Phi_{fs} = 0.1398 t_{CB}^{-0.66} H^{0.33} \quad (35a)$$

Or,

$$\Phi_{fs} = 0.1822 t_{CB}^{-0.44} H^{0.33} \quad (35b)$$

International Journal of Engineering Research & Technology (IJERT)
ISSN: 2278-0181
Vol. 7 Issue 12, December-2018

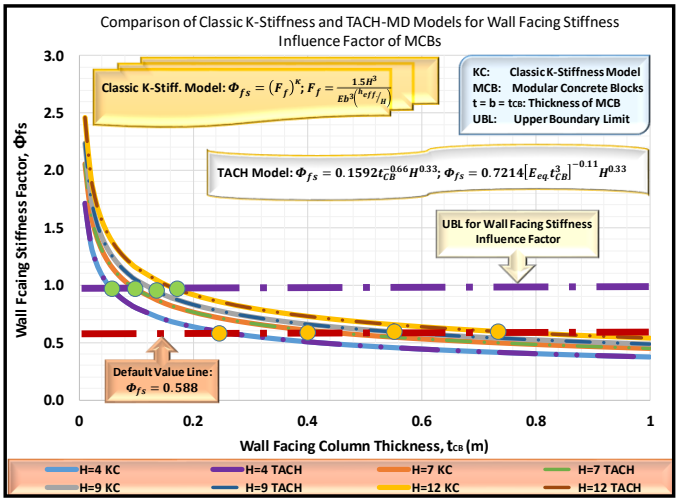

Fig. 24. Comparison between K-Stiffness and TACH-MD models for the wall facing stiffness influence factor.

The following observations can be made from Figure 24: i) the curves generated from both models show a perfect agreement (superimposition); ii) the contribution of the wall facing stiffness degrades with the increase in wall facing column thickness tending towards a residual state; iii) as expected, the degradation is critical (acute) for thinner walls within the range of; $t_{CB} < 0.06m$ for $H = 4m$ to $t_{CB} < 0.19m$ for $H = 12m$ implying that the rate of decay is also dependent upon the height of the GMSE-GRS wall; iv) the Upper Boundary Limit (UBL) clearly demarcates both the limit of the wall facing stiffness contribution and the end of critical degradation; and v) the default value line plotted at; $\Phi_{fs} = 0.588$, inidcates that this value is attained when the thickness is: $t_{CB} = 0.25m$ for $H = 4m$; $t_{CB} = 0.40m$ for $H = 7m$, $t_{CB} = 0.54m$ for $H = 9m$ and $t_{CB} = 0.73m$ for $H = 12m$.

3) Comparison of wall facing batter angle influence factor models

Figures 25 and 26 show the comparison of the results generated from the classic K-Stiffness and the TACH-MD models for the wall facing batter angle influence factor. Whilst Figure 25 depicts this comparison for the batter angle factor plotted as a function of the angle of internal friction of the reinforced backfill geomaterials and batter angle, Figure 26 makes a direct comparison of the two sets of data against the line of perfect superimposition. The K-Stiffness curves were generated from model Equation 13, whilst the ones for the TACH-MD model were generated from Equation 36.

$$\Phi_{fb} = -1.0967 \times 10^{-5}\omega^{0.9673}\phi_{rbf}'^{2} + 0.000275\phi_{rbf}' + 1.0001exp(-0.011\omega) \quad (36)$$

The results from these figures indicate that: i) perfect superimposition is achieved for both models as the batter angle becomes lower implying that the K-Stiffness model was calibrated for lower batter angles with an average of; ω = 11.5°, most of the walls of which were lower than this value (refer to the data in Tables III and VI); ii) the ω = 20°curves exhibit signicant deviation due to the reason given in i); note that the TACH-MD models were developed on the basis of a wider range of data; and iii) the magnitude and characteristics of the batter factor are significantly impacted by the shear strength of the reinforced backfill geomaterial whereby this influence increases with increase in the magnitude of the batter angle.

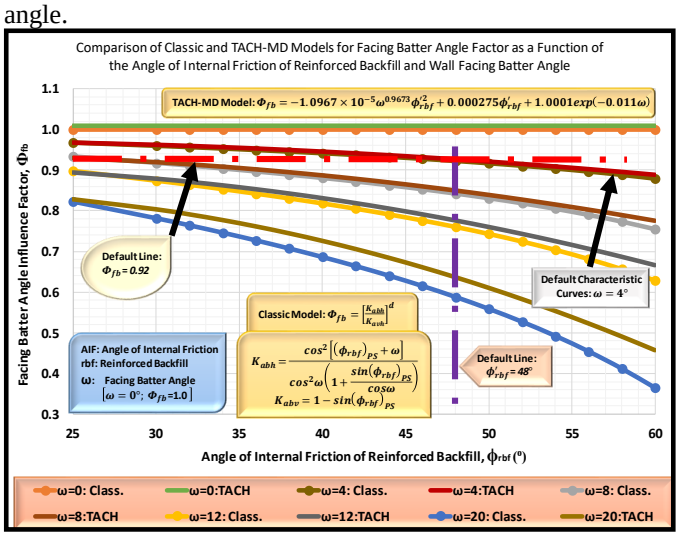

Fig. 25. Comparison between K-Stiffness and TACH-MD models for the wall facing batter angle influence factor as a function of the angle of internal friction of reinforced backfill and magnitude of wall facing batter angle.

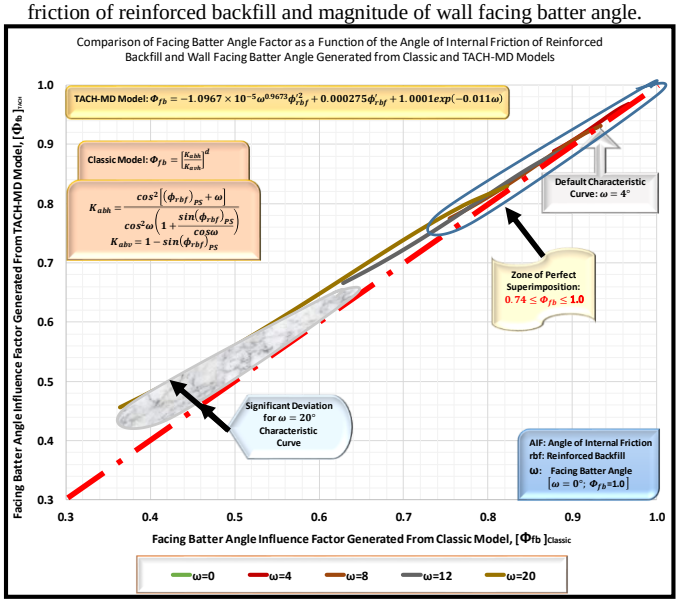

Fig. 26. Comparison between K-Stiffness and TACH-MD models for the wall facing batter angle influence factor as a function of the angle of internal friction of reinforced backfill and magnitude of wall facing batter angle.

4) Comparison of cohesion influence factor models

The influence factor that measures the contribution of cohesion to the magnitude of the maximum reinforcement load and other parameters is graphically plotted in Figures 27 and 28 for curves generated from both models. The data was generated adopting Equation 19 for the classic K-Stiffness model and Equations 37 and 38 for the TACH-MD model.

$$\Phi_c = 1 - 6.5 \times \frac{(C+C_{IR})}{\gamma_{rbf}HRF_{cc}} = 1 - 6.5 \times \frac{(C+C_{IR})}{14.673exp\left(0.0091\phi_{rbf}'\right)HRF_{cc}} \Bigg\| 5 \le (C + C_{IR}) \le 100kPa \quad (37)$$

$$\Phi_c = 1 - 0.1968H^{-1}exp\left(-0.0091\phi_{rbf}'\right) \times (C + C_{IR}) \quad (38)$$

International Journal of Engineering Research & Technology (IJERT)
ISSN: 2278-0181
Vol. 7 Issue 12, December-2018

where, $C_{IR} = 2.5815\rho_r^{0.6437}$; $\rho_r = \left(\frac{T_{ult.}}{S_v}\right) \times R_c$; C_{IR}: Reinforcement Induced Cohesion (RIC).

In this case, the reinforcement induced cohesion (RIC) was considered to be zero ($C_{IR} = 0$) since this factor is not incorporated in the classic K-Stiffness model.

The cohesion influence factor is plotted as a function of both the cohesion intercept and the quality of reinforced backfill geomaterials delineated in terms of shear strength (angle of internal friction/shearing resistance). The results in Figures 27 and 28 depict that: i) the curves exhibit perfect superimposition for both models; ii) the influence of cohesion reduces as the cohesion intercept increases; and iii) as the shear strength increases, the contribution of the cohesion influence factor is reduced.

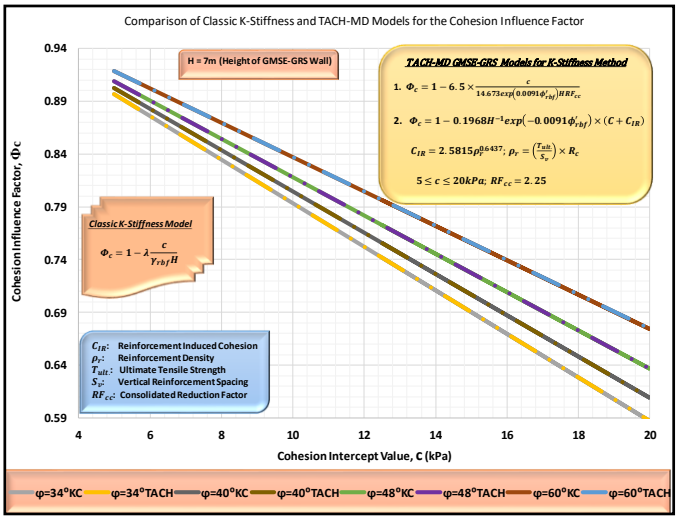

Fig. 27. Comparison between K-Stiffness and TACH-MD models for the cohesion influence factor as a function of the cohesion intercept value and angle of internal friction of reinforced backfill.

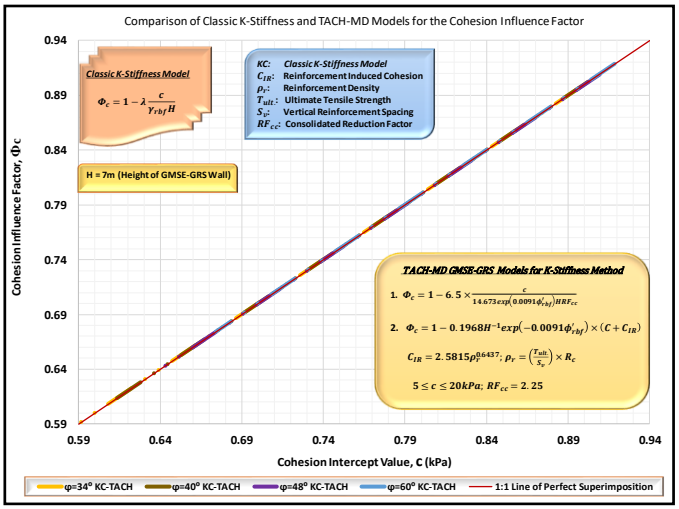

Fig. 28. Superimposition omparison between K-Stiffness and TACH-MD models for the cohesion influence factor as a function of the angle of internal friction of reinforced backfill.

IV. CORRELATION AND CHARACTERIZATION OF PRINCIPAL INFLUENCE FACTORS

Details under this topic are discussed in [2], which not only correlates all the principal influence factors but also provides particularization of their characteristics and quantification of their contribution to the internal stability of GMSE-GRS walls. Limited examples correlating the global, local and wall facing stiffness are subsequently presented.

A. *Correlating global and local stiffness influence factors*

The correlation between the global and local stiffness influence factors as a function of the wall height is depicted in Figure 29; the curves are generated from Equation 39.

$$\Phi_{local} = \{-170.85exp(0.023H)\Phi_g^2 + 119.48exp(-0.011H)\Phi_g - 20.1424\} \times \left[\frac{D_{tmax}}{D_{tmax}^{ref.}}\right] \quad (39)$$

The following derivations can be made from Figure 29: i) local stiffness increases with increasing global stiffness; ii) the rate of increase is higher for the local than the global stiffness factor; and iii) whilst the default value line for the local stiffness influence factor intersects all curves including $H = 4 \sim H = 30m$, the global one is limited to $H = 12m$, which is the limiting calibration height of the K-Stiffness Method.

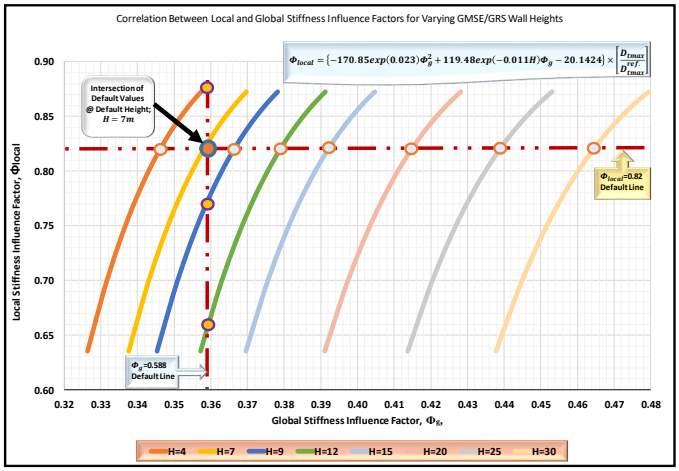

Fig. 29. Influence of GMSE-GRS wall column height and shear strength of reinforced backfill geomaterials on the cohesion influence factor.

B. *Correlating global and wall facing stiffness influence factors*

The reciprocal correlations of the global and wall facing stiffness influence factors are evaluated using Equations 40 and 41.

$$\Phi_g = 0.3143exp(0.0136H)\Phi_{fs}^{[-0.0601exp(0.0232H)]} \times \left[\frac{D_{tmax}}{D_{tmax}^{ref.}}\right] \quad (40)$$

$$\Phi_{fs} = exp\left\{[-0.0601exp(0.0232H)]^{-1} ln\left[\frac{\Phi_g}{(0.3143exp(0.0136H))}\right] \times \left[\frac{D_{tmax}^{ref.}}{D_{tmax}}\right]\right\} \quad (41)$$

V. PREDICTION AND CHARACTERIZATION OF THE MAXIMUM REIFORCEMENT LOAD

A. *Preamble*

Various TACH-MD GMSE-GRS universal models are proposed for defining and predicting the maximum reinforcement load. The models correlate the T_{max} to GMSE wall height, H and maximum reinforcement load distribution

International Journal of Engineering Research & Technology (IJERT)
ISSN: 2278-0181
Vol. 7 Issue 12, December-2018

factor, D_{tmax} to various other principal design parameters and influence factors including: i) angle of internal friction of the reinforced backfill, ϕ_{rbf}; ii) elastic modulus, E_0; iii) unit weight, γ_{rbf}; iv) coefficient of lateral pressure, K; v) ultimate tensile (index) strength, $T_{ult.}$; vi) ultimate load carrying capacity, $q_{ult.}$; vii) secant stiffness @ end of construction, J_{EOC}; viii) global stiffness influence factor, Φ_g(Equation 42); ix) local stiffness influence factor, Φ_{local}; x) wall facing stiffness influence factor, Φ_{fs}; xi) wall facing batter angle influence factor, Φ_{fb}; and xii) cohesion influence factor, Φ_c.

The TACH-MD GMSE-GRS universal models for i) ~ xii) are proposed in [3], which is the third part of this paper.

B. Influence of global stiffness and GMSE-GRS wall height on the maximum reinforcement load, Tmax

The application of the global stiffness factor and the GMSE-GRS wall height in the prediction of the maximum reinforcement load can be made by adopting model Equation 42; the converse of which can be evaluated using Equation 43.

$$T_{max} = exp\{-[0.0922exp(-0.033H)]^{-1}ln(3.4977H^{-0.1411}\Phi_g)\} \times \left[\frac{D_{tmax}^{ref.}}{D_{tmax}}\right] \quad (42)$$

$$\Phi_g = 0.2859H^{0.1411}T_{max}^{-[0.0922exp(-0.033H)]} \times \left[\frac{D_{tmax}}{D_{tmax}^{ref.}}\right] \quad (43)$$

Figure 30 shows that: i) the upper and lower boundary values of the maximum reinforcement load are primarily dictated by height of the GMSE-GRS wall with the resulting T_{max} increasing with the increase in height; and ii) for $H \leq 12m$; $T_{max} \leq 8\,kN/m$ (walls calibrated for K-Stiffness).

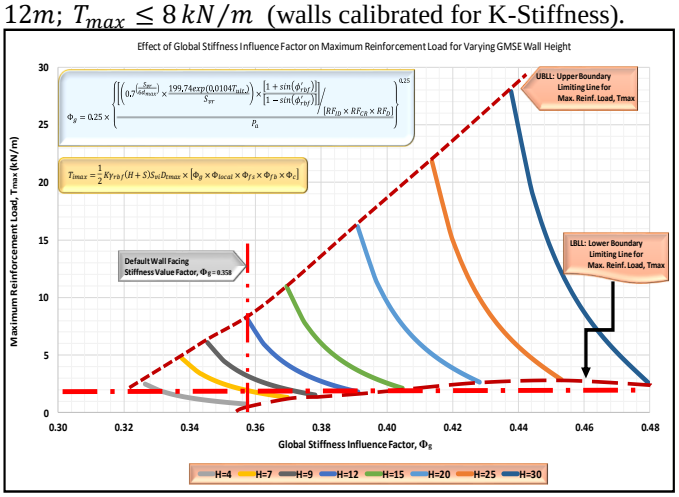

Fig. 30. Application of GMSE-GRS wall height and wall facing stiffness factor in the prediction of the maximum reinforcement/tensile load.

C. Variation of maximum load distribution factor with GMSE-GRS wall depth under the influence of the angle of internal friction (shearing resistance)

The results generated using Equation 44 are graphically plotted in Figure 31. The model is useful in predicting the value of the critical failure characteristics and the maximum reinforcement load distribution factor.

$$D_{tmax} = 0.858H^{0.234} \times \left[356.81\phi_{rbf}^{\prime -1,829} \times H^{\left(4\times10^{-5}\phi_{rbf}^{\prime 2}-0.0023\phi_{rbf}^{\prime}+0.3643\right)}\right]^{(0.6283H^{0.2792})} \quad (44)$$

It can be inferred from Figure 31 that: i) maximum reinforcement load distribution characteristics are highly dependent on the shear strength of the reinforced backfill (RBF) geomaterial; ii) RBF geomaterials with friction angles of $\phi_{rbf}^{\prime} \leq 34°$ can only be characterized by the D_{tmax} factor for GMSE-GRS walls that are below 3m in height ($H \leq 3m$) whereas, for the default value of $\phi_{rbf}^{\prime} = 48°$, the D_{tmax} factor can be adopted for walls up to; $H = 12m$, which is the limiting height of the K-Stiffness Method; and iii) the default value for the D_{tmax} factor can graphically be confirmed to be; $D_{tmax} = 0.7$. Also refer to the subsequent Section VI. for further insight on the influence of the shear strength of RBF geomaterials.

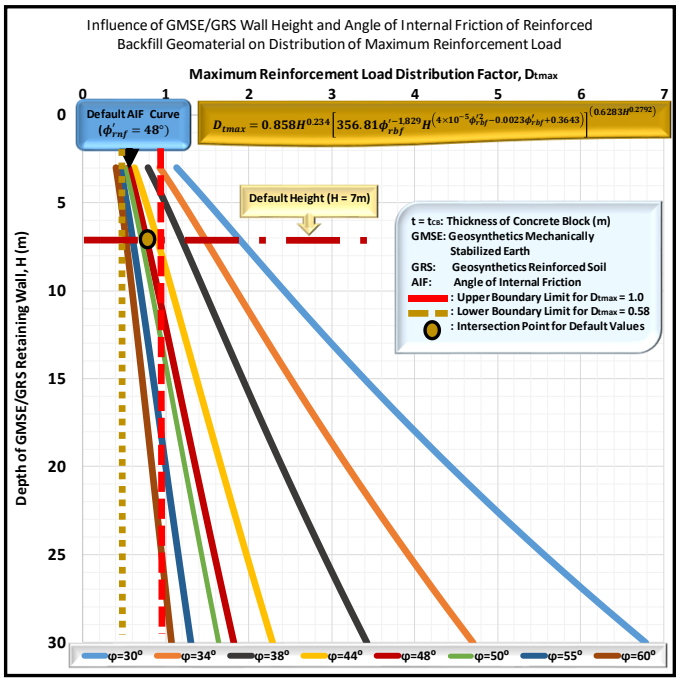

Fig. 31. Influence of GMSE-GRS wall height and shear strength of reinforced backfill geomaterial on the distribution of the maximum reinforcement load.

VI. INFLUENCE OF QUALITY OF REINFORCED BACKFILL GEOMATERIALS ON THE INTERNAL STABILITY OF GMSE-GRS RETAINING WALLS

The quality of reinforced backfill geomaterial is evaluated mainly on the basis of the physical and mechanical properties including the angle of internal friction/shearing resistance, $\phi_{rbf}^{\prime}$, unit weight, γ_{rbf}, stiffness defined in terms of small strain elastic modulus, E_0, cohesion intercept, c and index parameters, mainly plasticity index, P_I. Whilst limited examples that validate the influence of quality of reinforced backfill geomaterials are subsequently provided, the details regarding the same are discussed methodically in [4].

A number of researchers have shown that the type of backfill had the most profound effect on various aspects of the behavior and performance of the GMSE-GRS geostructures ([14], [15], [16] and [42]). Also refer to Section VIII.

A. Influence of RBF geomaterial properties and GMSE-GRS wall height on the global stiffness factor

One of the TACH-MD models that is applicable in demonstrating the effect of the quality of the reinforced

International Journal of Engineering Research & Technology (IJERT)
ISSN: 2278-0181
Vol. 7 Issue 12, December-2018

backfill geomaterial and GMSE-GRS wall height on the global stiffness factor is defined in Equation 45.

$$\Phi_g = 0.3143exp(0.0136H) \times \left\{356.81\phi_{rbf}'^{-1.829}H^{\left(4\times10^{-5}\phi_{rbf}'^{2}-0.0023\phi_{rbf}'+0.3643\right)}\right\}^{[-0.0601exp(0.0232H)]} \left[\frac{D_{tmax}}{D_{tmax}^{ref.}}\right] \quad (45)$$

B. Influence of RBF geomaterial properties and GMSE-GRS wall height on the equivalent wall facing stiffness factor

Equations 46 and 47 are adopted in characterizing the influence of RBF geomaterial properties on the equivalent wall facing stiffness influence factor as a function of GMSE-GRS wall height. The results generated using this equation are graphically plotted in Figure 32.

$$\Phi_{fs} = \left\{0.1592\left[455.25\phi_r'^{-2.771} \times H^{\left(6\times10^{-5}\phi_r'^{2}-00035\phi_r'+1.052\right)}\right]^{-0.66}H^{0.33}\right\}^{-1} \quad (46)$$

$$\Phi_{fs} = 356.81\phi_{rbf}'^{-1.829}H^{\left(4\times10^{-5}\phi_{rbf}'^{2}-0.0023\phi_{rbf}'+0.3643\right)} \quad (47)$$

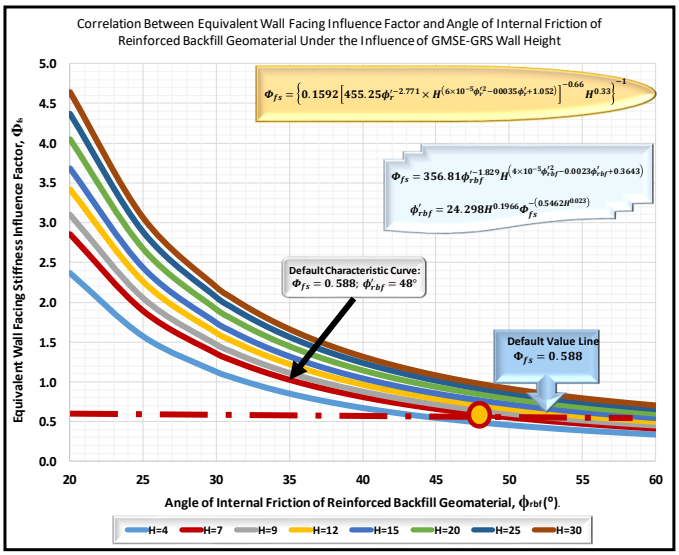

Fig. 32. Influence of quality of reinforced backfill geomaterial defined in terms of shear strength (angle of internal friction) and GMSE-GRS wall height on the equivalent wall facing stiffness influence/contribution.

The characteristic curves depicted in Figure 32 show that: i) the equivalent wall facing stiffness increases with increasing magnitude of shearing resistance; ii) the contribution of the wall facing stiffness influence factor degrades as the GMSE-GRS height increases; and iii) it can be derived that the influence of the equivalent wall facing stiffness factor is effectively initiated when: $\phi_{rbf}' = 34°\ for\ H = 4m$, $\phi_{rbf}' = 36°\ for\ H = 7m$, $\phi_{rbf}' = 40°\ for\ H = 12m$, whilst $\phi_{rbf}' = 50°\ for\ H = 30m$, values which constitute the lower boundary limits of the required angle of internal friction.

C. Influence of RBF geomaterial quality and GMSE-GRS wall height on the maximum reinforcement load

The influence of reinforced backfill geomaterial quality on the maximum reinforcement load can be investigated through the use of the analytical model defined in Equation 48.

$$T_{max} = \left\{0.8103H^{1.3058}exp\left[-(1\times10^{-4}H^2 - 0.0003H + 0.0317)\phi_{rbf}'\right]\right\} \times \left[\frac{D_{tmax}}{D_{tmax}^{ref.}}\right] \quad (48)$$

The results generated using Equation 48 are illustrated in Figure 33. It can be seen that the shear strength of the backfill defined in terms of the angle of internal friction/shearing resistance has significant influence on the magnitude and characteristics of the maximum reinforcement load (MRL). It can further be derived that the resulting MRL reduces exponentially as the shear strength increases and that this characteristic is also considerably impacted by the height of the GMSE-GRS wall.

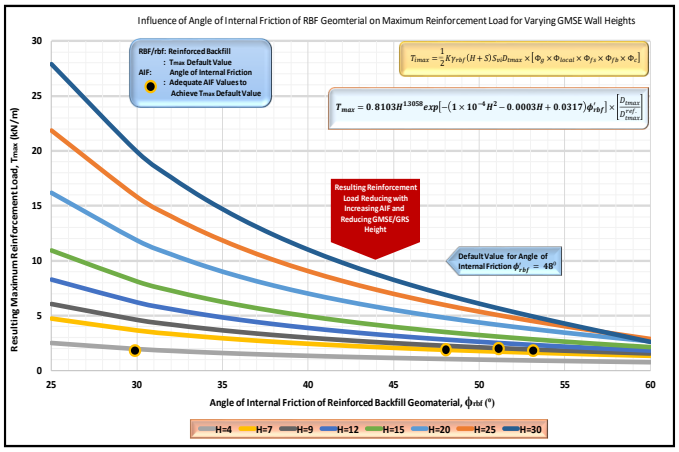

Fig. 33. Influence of quality of reinforced backfill geomaterial defined in terms of shear strength (angle of internal friction) and GMSE-GRS wall height on the maximum reinforcement load.

D. Influence of RBF geomaterial properties, GMSE-GRS wall column thickness and batter angle on the geosynthetics base design length

One of the useful models in investigating the influence of RBF on principal internal stability design parameters is defined in Equation 49, the results of which are presented in Figure 34.

$$L_{GD}^{req} = 1.229 \times \left\{[0.0012\omega - 0.544]ln\left(\phi_{rbf}'\right) + 0.0044\omega + 1.7112\right\} \times H \quad (49)$$

International Journal of Engineering Research & Technology (IJERT)
ISSN: 2278-0181
Vol. 7 Issue 12, December-2018

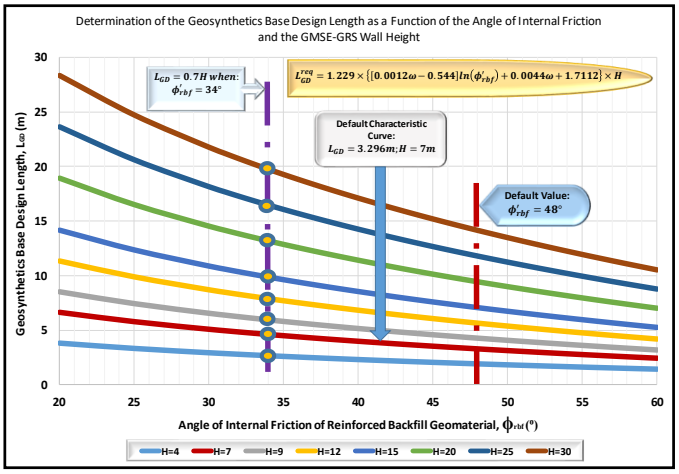

Fig. 34. Influence of quality of reinforced backfill geomaterial defined in terms of shear strength (angle of internal friction) and GMSE-GRS wall height on the required geosynthetics base design length.

The results in Figure 34, for a vertical GMSE-GRS wall $[\omega = 90 - \theta\ (\theta = 0)]$ clearly indicate that the angle of internal friction has ramarkable effects on the geosynthetics base design length. The plot further shows that the required base design length is reduced as the shear strength of the RBF increases and the GMSE-GRS wall height reduces. Another interesting derivation is the fact that the popularly adopted estimate; $(L_{GD} = 0.7H)$ is only valid when; $(\phi'_{rbf} = 34°)$ as demonstrated by the yellow marks with blue rings.

VII. Influence of Ultimate Load Carrying Capacity and Global Stiffness of Composite GMSE-GRS Mass on Internal Stability

The influence of ultimate load carrying capacity (ULCC) and global stiffness of the composite GMSE-GRS mass on the internal stability is punctiliously evaluated in [5]. An example of such application based on Equation 50 is provided in Figure 35. That ULCC has significant effect on the characteristics of the maximum reinforcement load can very well be appreciated.

$$T_{max} = \left\{[0.5741ln(H) - 0.2969]exp\left[\left(7 \times 10^{-5}H^2 - 0.0007H + 0.0342\right)\frac{q_{ult.,lc}}{\left[2.1257exp\left(0.0452\phi'_{rsf}\right)\right]}\right]\right\} \times \left[\frac{D_{tmax}}{D_{tmax}^{ref.}}\right] \quad (50)$$

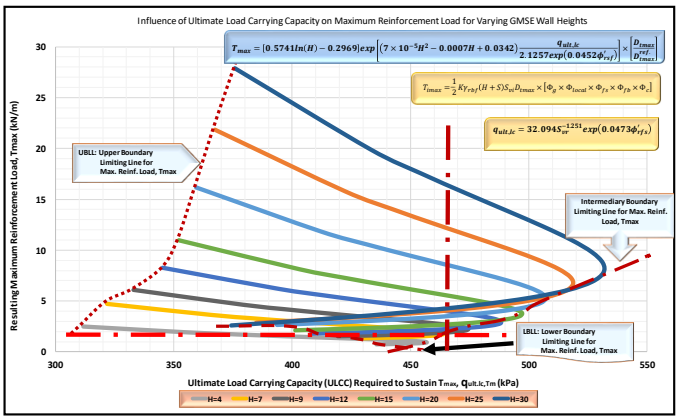

Fig. 35. Influence of ultimate load carrying capacity on the maximum reinforcement load for varying GMSE-GRS wall heights.

VIII. Seismic Analysis in Cogitation of the K-Stiffness Influence Factors and Parametric Variability

The inimitable TACH-MD analytical models that are applicable in carrying out rigorous seismic analysis in cogitation of the influence factors proposed in the K-Stiffness Method and a wide range of parametric variability are conscientiously examined in [6]. The models have also been developed to enable profound seismic analysis in rumination of reciprocal parametric effects (refer to Section III for validation).

Some of integral aspects ruminated include the seismic effects and/or interactive features regarding/involving: i) the influence factors introduced in the K-Stiffness working stress Method that mainly take into account, the structural contribution of global and local stiffness, wall facing rigidity, batter angle and cohesion (reinforced backfill geomaterial properties), among other minor factors; ii) precise prediction and optimal quantification of the maximum reinforcement load and its' distribution thereof; iii) reinforcement stiffness; iv) serviceability limit state; v) characteristics of yield and connection strengths of the reinforcing elements; vi) distribution attributes of the peak horizontal acceleration within the reinforced soil zone for varying magnitudes of reinforcement stiffness, wall geometry and quality of backfill geomaterials; vii) principal geosynthetics-soil interactive design parameters mainly the base design length and vertical reinforcement spacing; and viii) damping characteristics, among other considerations [43]. A few examples of this initiative are provided in the subsequent sub-Sections A. ~ D.

A. Influence of GMSE-GRS wall geometry and reinforced backfill geomaterial properties on the force coefficient, K

The TACH-MD analytical model that can be used for reconnoitering the impact of GMSE-GRS wall geometry and quality of reinforced backfill geomaterials can be undertaken adopting Equation 30 (model is inset in Figure 36). The graphical curves depicted in Figure 36 were generated using this equation. It can be discerned that both these parameters have a linear influence on the seismic force coefficient as has been reported by various researchers ([39], [40], [44]). It can also be observed that as the shear strength of the reinforced backfill, ϕ'_{rbf} increases the wall facing thickness to height ratio, t/H tends to a limiting value within the 1st quadrant.

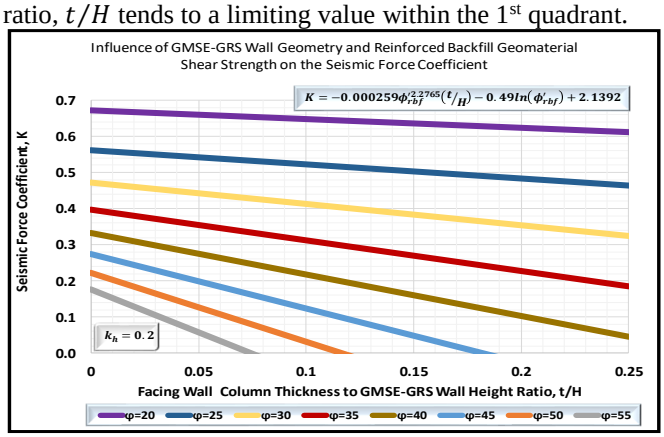

Fig. 36. Influence of quality of reinforced backfill geomaterial defined in terms of shear strength (angle of internal friction) and GMSE-GRS wall geometry on the seismic force coefficient: TACH-MD modelled results (refer to validation in Figure 18).

International Journal of Engineering Research & Technology (IJERT)
ISSN: 2278-0181
Vol. 7 Issue 12, December-2018

B. Influence of seismic acceleration and reinforced backfill geomaterial properties on seismic coefficient of active pressure

The influence of seismic acceleration and quality of reinforced backfill can be explored by employing model Equations 31and 32. The results presented in Figure 37 demonstrate that both these parameters have significant effects on the magnitude and characteristics of the coefficient of seismic earth pressure whereby an increase in the quality of geomaterials (angle of internal friction/shearing resistance) culminates in a reduction of the resulting earth pressure whereas the converse applies to the seismic acceleration.

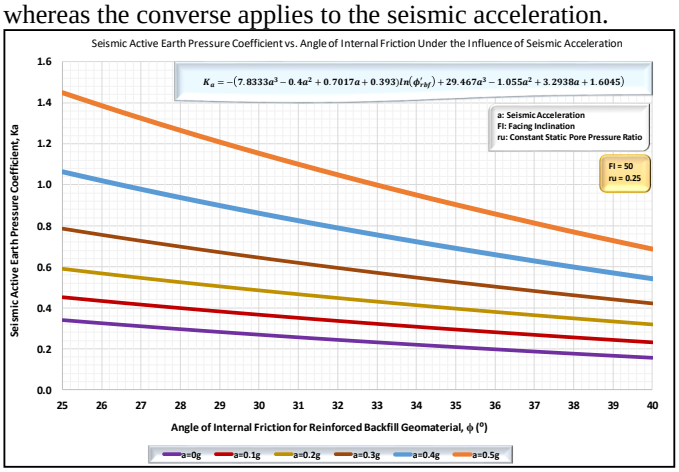

Fig. 37. Influence of quality of reinforced backfill geomaterial defined in terms of shear strength (angle of internal friction) and seismic acceleration on the coefficient of seismic earth pressure: TACH-MD modelled results (refer to validation in Figure 19).

C. Influence of GMSE-GRS wall geometry and wall facing stiffness influence factor on the force coefficient, K

As one of the vast examples to be presented and discussed comprehensively in [6], which involve the influence factors proposed in the K-Stiffness Method, the models delineated in Equations 51 ~ 53 and the corresponding results plotted in Figures 38 and 39 are invoked accordingly.

$$K = -0.000259\left[24.298H^{0.1966}\Phi_{fs}^{-(0.5462H^{0.023})}\right]^{2.2765}\left(t/H\right) - 0.49ln\left[24.298H^{0.1966}\Phi_{fs}^{-(0.5462H^{0.023})}\right] + 2.1392 \quad (51)$$

The characteristic curves depicted in Figure 38 represent the degree of influence of the wall facing stiffness factor on the magnitude of the seismic force coefficient for varying wall facing column thickness to GMSE-GRS wall height ratio (t/H). The following derivations can be made from this figure: i) the influence of the wall facing stiffness factor is definitively significant; ii) the force coefficient increases in exponential proportion with the increase in Φ_{fs}; iii) reduction in the t/H ratio results in increased seismic force; iv) the default seismic force coefficient value can be designated as: $K = 0.167$ for a GMSE-GRS height of $H = 7m$ and $\Phi_{fs} = 0.588$; and v) the proposed model can be effectively adopted for the intended purposes.

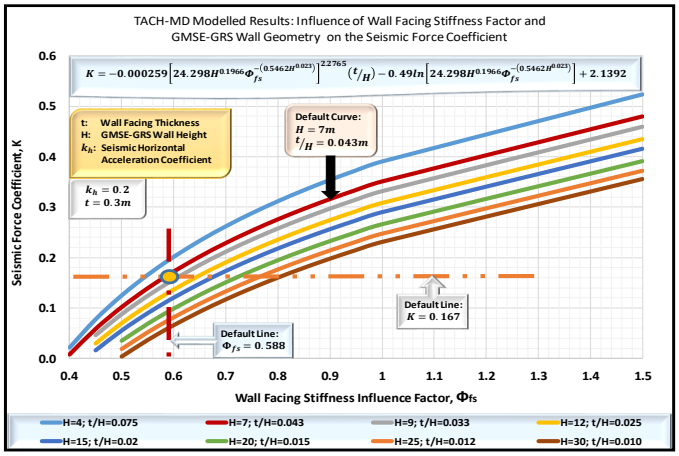

Fig. 38. Influence of wall facing stiffness factor and GMSE-GRS wall geometry on the seismic force coefficient: TACH-MD modelled results.

D. Influence of the wall facing stiffness influence factor on the seismic active earth pressure coefficient for varying magnitudes of seismic acceleration.

The influence of the wall facing stiffness factor on the seismic active earth pressure coefficient for varying magnitudes of seismic acceleration can be investigated through the application of the models delineated in Equations 52 and 53; for estimation and perfect fit solutions, respectively. The graph depicted in Figure 39 is plotted using Equation 53. This figure demonstrates that the wall facing stiffness influence factor has considerable impact on the magnitude and characteristics of the resulting seismic active earth pressure coefficient notwithstanding the scale of the seismic acceleration. Nevertheless, it can be inferred that the degree of this influence is impacted by the magnitude of seismic acceleration.

$$K_a = -0.3818exp(2.2693a)ln\left[24.298H^{0.1966}\Phi_{fs}^{-(0.5462H^{0.023})}\right] + 1.5686exp(2.3868a) \quad (52)$$

$$K_a = -(7.8333a^3 - 0.4a^2 + 0.7017a + 0.393))ln\left[24.298H^{0.1966}\Phi_{fs}^{-(0.5462H^{0.023})}\right] + 29.467a^3 - 1.055a^2 + 3.2938a + 1.6045 \quad (53)$$

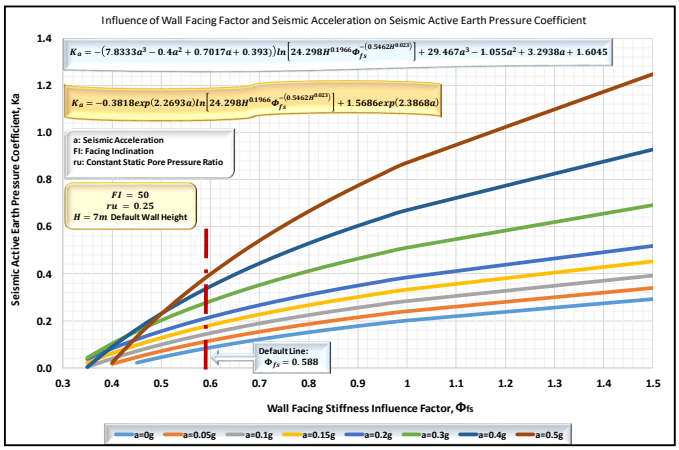

Fig. 39. Influence of wall facing stiffness factor and seismic acceleration on the seismic active earth coefficient: TACH-MD modelled results.

International Journal of Engineering Research & Technology (IJERT)
ISSN: 2278-0181
Vol. 7 Issue 12, December-2018

IX. APPLICATION OF PROPOSED TACH-MD GMSE-GRS ANALYTICAL MODELS IN DESIGN AND STABILITY ANALYSES

Application of the proposed TACH-MD GMSE-GRS analytical models is to be discussed in detail in [7]. As can be derived, the analytical models expressed in Equations 54 and 55 correlating the maximum reinforcement load, T_{max} to the geosynthetic base design length, L_{GD} and the vertical reinforcement spacing, S_v, respectively; as a function of GMSE-GRS wall height, H can be adopted in the prediction and characterization of T_{max}. Note that the L_{GD} and S_v are most integral parameters in relation to the internal stability design. The results generated from these models are depicted in Figures 40 and 41 for the T_{max}~L_{GD} and T_{max}~S_v, respectively.

$$T_{max} = \left\{[0.4846ln(H) - 0.3888]exp\left[(0.0007H^2 - 0.0284H + 2.5028)\frac{L_{GD}}{H}\right]\right\} \times \left[\frac{D_{tmax}}{D^{ref.}_{tmax}}\right] \quad (54)$$

$$T_{max} = \left\{[0.4846ln(H) - 0.3888]exp\left[(0.0007H^2 - 0.0284H + 2.028)\left[21.796exp\left[-0.055\phi'_{rbf}\right]S_v^{2.1268}\right]\right]\right\} \times \left[\frac{D_{tmax}}{D^{ref.}_{tmax}}\right] \quad (55)$$

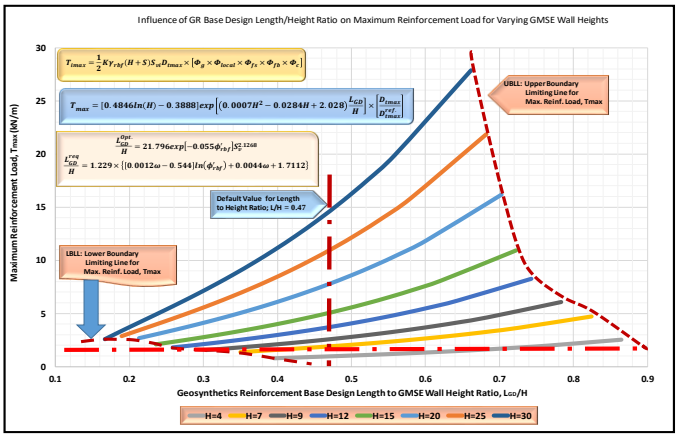

Fig. 40. Correlation between maximum reinforcement load, T_{max} and geosynthetics-soil interaction principal design parameter (base design length, L_{GD} as a function of GMSE-GRS wall height.

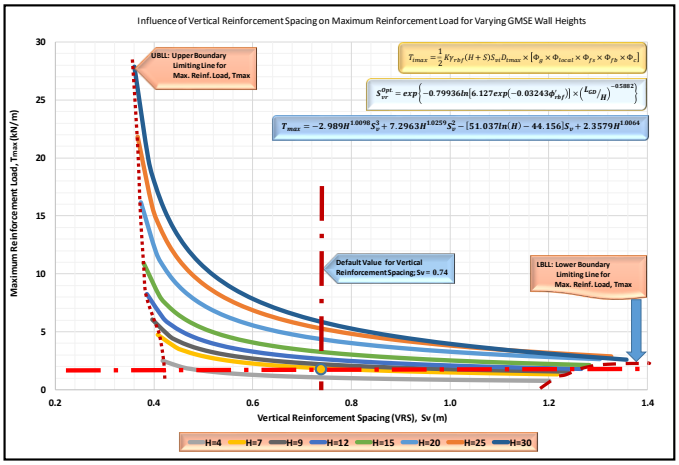

Fig. 41. Correlation between maximum reinforcement load, T_{max} and geosynthetics-soil interaction principal design parameter (vertical reinforcement spacing, S_v) as a function of GMSE-GRS wall height.

X. ESTABLISHMENT OF APPROPRIATE SERVICEABILITY CRITERIA AND PREDICTION OF STRUCTURAL PERFORMANCE

Reference [8] proposes and delineates analytical models that can be applied to establish the appropriate serviceability criteria depending on various prevalent conditions and variables. Analytical models that can be adopted in the prediction of the structural performance of GMSE-GRS geostructures are also proposed and discussed herein. Equations 56 ~ 58 and Figures 42 and 43 provide but a few of such applications ([45], [46]).

A. Universal model correlating maximum lateral deflection to wall facing stiffness factor, GMSE-GRS wall height and shear properties of reinforced backfill geomaterial

Equation 56 defines the analytical universal model correlating the maximum lateral deflection to the wall facing stiffness influence factor, GMSE-GRS wall height and the shear properties of reinforced backfill geomaterial.

$$\delta_{h,max} = 0.813exp\left\{-0.65\left[0.2106\left(exp\left(-1.5151515ln\left(\frac{7.1531\Phi_{fs}}{H^{0.33}}\right)\right)\Big/_{H}\right) - 0.0001\right] \times e^{0.0783\phi'_{rbf}}\right\} \times H^{2.0624}\ (mm) \quad (56)$$

B. Influence of wall facing stiffness on structural performance and serviceability limit state

The results depicted in Figure 42 indicate that the maximum lateral deflection is defined by both the wall facing stiffness, Φ_{fs} and the height of the GMSE-GRS wall, H.

$$\delta_{h,max} = \frac{[0.7545H^2 + 0.3259H + 6.325]}{\left[1 + exp\left\{-1.5151515ln\left[\frac{7.1531\Phi_{fs}}{H^{0.33}}\right]\right\}\right]}\ (mm) \quad (57)$$

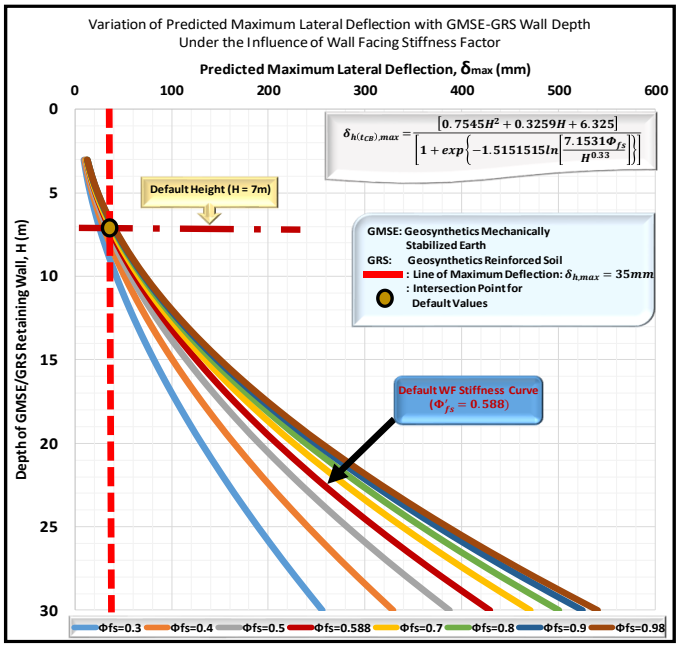

Fig. 42. Variation of predicted maximum lateral deflection, δ_{max} with depth of GMSE-GRS walls considering effects of the wall facing stiffness factor, Φ_{fs}.

International Journal of Engineering Research & Technology (IJERT)
ISSN: 2278-0181
Vol. 7 Issue 12, December-2018

C. Nomograph for designating maximum deflection in relation to wall facing stiffness influence factor with GMSE-GRS wall structural thickness considerations

Figure 43 is cogitated to be a useful nomograph for specifying the maximum lateral deflection based on the magnitude of the wall facing stiffness influence factor as a function of the wall facing thickness. This figure clearly shows that the wall facing stiffness significantly impacts on the magnitude of lateral deflection and that the degree of this influence is highly dependent upon the thickness of the wall facing column.

$$\Phi_{fs} = 0.1439 t_{CB}^{-0.607} \delta_{h_{max}}^{0.1871} \quad (58)$$

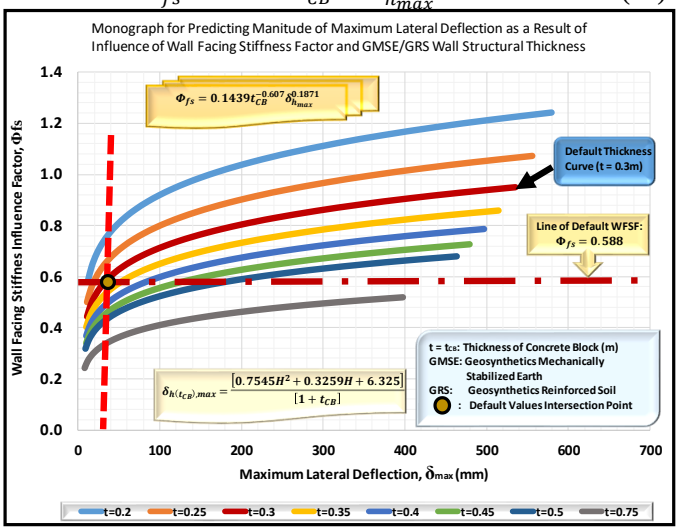

Fig. 43. Nomograph for predicting the magnitude of maximum lateral deflection under the influence of wall facing stiffness factor and GMSE-GRS structural thickness.

XI. CONCLUSIONS

Universal and versatile analytical models equipped with a variety of application modules have been proposed in this paper. Application of the proposed models has been practically manifested through graphical examples for the characterization of the influence factors and material properties as well generation of imperative design parameters. The design characteristic curves and parametric values generated based on the application of these models distinctly confirm the validity, lucidity and rationality of the proposed analytical models. In particular, the following conclusions can be derived.

1. The proposed TACH-MD GMSE-GRS analytical models developed for the K-Stiffness Method geo-mathematically confirm the validity of the influence factors and facilitate for their versatile application and parametric correlation.
2. The upper and lower boundary values of the maximum reinforcement load are primarily dictated by height of the GMSE-GRS wall with the resulting T_{max} increasing with the increase in height; and that for $H \leq 12m$; $T_{max} \leq 8\,kN/m$ in conformity with the results reported for the walls calibrated for the K-Stiffness Method.
3. The maximum reinforcement load distribution characteristics are highly dependent on the shear strength of the reinforced backfill (RBF) geomaterial; and that RBF geomaterials with friction angles of $\phi'_{rbf} \leq 34°$ can only be characterized by the D_{tmax} factor for GMSE-GRS walls that are below 3m in height $(H \leq 3m)$ whereas, for the default value of $\phi'_{rbf} = 48°$, the D_{tmax} factor can be adopted for walls up to; $H = 12m$, which is the limiting height of the K-Stiffness Method.
4. The equivalent wall facing stiffness increases with increasing magnitude of shearing resistance, whilst the contribution of the wall facing stiffness influence factor degrades as the GMSE-GRS height increases.
5. The influence of the equivalent wall facing stiffness factor is effectively initiated when: $\phi'_{rbf} = 34° \; for \; H = 4m$, $\phi'_{rbf} = 36° \; for \; H = 7m$, $\phi'_{rbf} = 40° \; for \; H = 12m$, whilst $\phi'_{rbf} = 50° \; for \; H = 30m$, values which constitute the lower boundary limits of the required angle of internal friction.
6. The shear strength of the backfill has significant influence on the magnitude and characteristics of the maximum reinforcement load.
7. The angle of internal friction has remarkable effects on the geosynthetics base design length whereby the required base design length is reduced as the shear strength of the RBF increases and the GMSE-GRS wall height reduces. Another interesting derivation is the fact that the popularly adopted estimate; $(L_{GD} = 0.7H)$ is only valid when; $(\phi'_{rbf} = 34°)$ as demonstrated in this paper.
8. That ultimate load carrying capacity has significant effect on the magnitude and characteristics of the maximum reinforcement load.
9. The influence of the wall facing stiffness factor on the force coefficient is definitively significant; implicit that increased facing stiffness exponentially reduces the force coefficient.
10. The wall facing stiffness influence factor has considerable impact on the magnitude and characteristics of the resulting seismic active earth pressure coefficient notwithstanding the scale of the seismic acceleration, the extent of which is dependent on the magnitude of seismic acceleration.
11. The influence factors have profound impact on the geosynthetic base design length, L_{GD} and the vertical reinforcement spacing, S_v parameters of which are most integral in relation to the internal stability design.
12. The results depicted in Figure 42 indicate that the maximum lateral deflection is defined by both the wall facing stiffness, Φ_{fs} and the height of the GMSE-GRS wall, H.
13. Figure 43 is cogitated to be a useful nomograph for specifying the maximum lateral deflection based on the magnitude of the wall facing stiffness influence factor as a function of the wall facing thickness. This figure clearly shows that the wall facing stiffness significantly impacts on the magnitude of lateral deflection and that the degree of this influence is highly dependent upon the thickness of the wall facing column.
14. It is pragmatically demonstrated that the models proposed in this paper have the propensity to enable probing of limits and the extrapolated application of the

International Journal of Engineering Research & Technology (IJERT)
ISSN: 2278-0181
Vol. 7 Issue 12, December-2018

K-Stiffness Method to transcend the existing limitations including seismic response analysis.

15. The proposed analytical models can be effectively used in determining the appropriate limiting boundaries of the batter angle as a function of the shear strength of the reinforced backfill geomaterial and in modelling and determining the parameters required to achieve an optimal internal stability design mainly in consideration of the influence factors and various other design parameters.

ACKNOWLEDGMENT

The author wishes to acknowledge, with utmost gratitude, Prof. Richard Bathurst and Prof. Fumio Tatsuoka for kindly sharing their research, which have provided exceptional insight in the comprehension and elucidation of the internal stability characteristics.

Sincere appreciation is also expressed to the Japan International Cooperation Agency (JICA), Japan Bank of International Cooperation (JBIC), Construction Project Consultants Inc., Kajima Corporation and Kajima Foundation for funding a substantial part of the study conducted in Africa. The author is also indebted to the Materials Testing & Research Department, Ministry of Transport & Infrastructure, Kenya, as well as the Research Teams of Kensetsu Kaihatsu Engineering Consultants Limited and the Kenya Geotechnical Society (KGS) for their relentless efforts in providing the due assistance that culminated in the successful compilation of this paper.

REFERENCES

[1] Allen, T.M., Bathurst, R.J., Holtz, R.D., Walters, D., and Lee, W.F. 2003. A new working stress method for prediction of reinforcement loads in geosynthetic walls. Canadian Geotechnical Journal, **40**(5): 976–994. doi:10.1139/t03-051.

[2] J.N. Mukabi, "Correlation and characterization of principal influence factors for internal stability design of GMSE-GRS geostructures", unpublished.

[3] J.N. Mukabi, "Prediction and characterization of maximum reinforcement loads for design of internal stability of GMSE-GRS geostructures", unpublished.

[4] J.N. Mukabi, "Influence of quality of reinforced backfill geomterials on the internal stability of GMSE-GRS geostructures", unpublished.

[5] J.N. Mukabi, "Evaluation of load carrying capacity and global stiffness of GMSE-GRS mass for internal stability design", unpublished.

[6] J.N. Mukabi, "Versatile analytical models for seismic analysis in cogitation of the K-Stiffness influence factors for internal stability of GMSE-GRS geostructures", unpublished.

[7] J.N. Mukabi, "Application of proposed versatile analytical models for advanced design of internal stability of GMSE-GRS geostructures", unpublished.

[8] J.N. Mukabi, "Designation of appropriate serviceability criteria and prediction of structural performance of GMSE-GRS geostructures", unpublished.

[9] Leshchinsky, D. and Han, J. 2003. Reinforced multitiered walls, Report DCT 158. Delaware Center for Transportation, University of Delaware, Newark, Delaware, USA.

[10] R.J. Bathurst, T.M. Allen and B.Q. Huang, "Current issues for the internal stability design of geosynthetic reinforced soil", proceedings 9th International Conference on geosynthetics, 2010.

[11] Christopher, B.R., Gill, S.A., Giroud, J.-P., Juran, I., Mitchell, J.K., Schlosser, F., and Dunnicliff, J. 1990. Reinforced soil structures. Vol. 1. Design and construction guidelines. Federal Highway Administration, Washington, D.C. FHWA Report FHWA-RD-89-043.

[12] Allen, T.M., and Bathurst, R.J. 2002*a*. Soil reinforcement loads in geosynthetic walls at working stress conditions. Geosynthetics International, **9**(5–6): 525– 566.

[13] AASHTO. 2002. Standard specifications for highway bridges. 17th ed. American Association of State Highway and Transportation Officials (AASHTO), Washington, D.C.

[14] J.N. Mukabi, "Inimitable Approach to design of foundations for GMSE and GRS retaining walls based on a case example", Proceedings of the 3rd World Congress on Civil, Structural and Environmental Engineering, Budapest, Hungary, 2018.

[15] J .N. Mukabi, "Profound methodology for prediction and evaluation of performance of GRE walls for road embankment and bridge abutments", *Proceedings of the XXVth World Road Congress*, Seoul, South Korea, November 2015, CD-Rom.

[16] J.N. Mukabi, "Proposed unique quasi-mechanistic models for advanced design of GMSE and GRS retaining wall geo-structures", Proceedings of the 3rd World Congress on Civil, Structural and Environmental Engineering, Budapest, Hungary, 2018.

[17] Bathurst, R.J., Miyata, Y., Nernheim, A. and Allen, T.M. 2008c. Refinement of K-stiffness Method for geosynthetic reinforced soil walls, Geosynthetics International, Vol. 15(4), pp. 269-295.

[18] Allen, T.M. and Bathurst, R.J. 2002. Soil reinforcement loads in geosynthetic walls at working stress conditions, Geosynthetics International, Vol. 9(5-6), pp. 525-566.

[19] Rowe, R.K., and Ho, S.K. 1993. A review of the behavior of reinforced soil walls. (Keynote Lecture.) In Earth reinforcement practice. Balkema, Rotterdam. pp. 801–830.

[20] Zornberg, J.G., Sitar, N., and Mitchell, J.K. 1998*a*. Performance of geosynthetic reinforced slopes at failure. Journal of Geotechnical and Geoenvironmental Engineering, ASCE, **124**(8): 670–683.

[21] Zornberg, J.G., Sitar, N., and Mitchell, J.K. 1998*b*. Limit equilibrium as basis for design of geosynthetic reinforced slopes. Journal of Geotechnical and Geoenvironmental Engineering, ASCE, **124**(8): 684–698.

[22] J.N. Mukabi, S.K. Kogi, M. Ndeda, J. Mbarua, G. Ogutu, E. Muthoka and S. K. Mukabi, "Webuye Interchange geotechnical engineering & foundation research report", *E-publication on Researchgate and Academia Websites*, 2018.

[23] Lade, P.V., and Lee, K.L. 1976. Engineering properties of soils. Report UCLA-ENG-7652, University of California, Los Angeles, California.

[24] Bolton, M.D. 1986. The strength and dilatancy of sands. Géotechnique, **36**(1): 65–78.

[25] Jewell, R.A., and Wroth, C.P. 1987. Direct shear tests on reinforced sand. Géotechnique, **37**(1): 53–68.

[26] Holtz, R.D., and Kovacs, W.D. 1981. An introduction to geotechnical engineering. Prentice-Hall Inc., Englewood Cliffs, N.J.

[27] Bathurst, R.J., Allen, T.M., and Walters, D.L. 2005. Reinforcement loads in geosynthetic walls and the case for a new working stress design method. Geotextiles and Geomembranes, **23**(4): 287–322. doi:10.1016/j.geotexmem.2005. 01.002.

[28] WSDOT. 2005. WSDOT standard practice T925: Standard practice for determination of long-term strength for geosynthetic reinforcement, Washington State Department of Transportation (WSDOT), Olympia, Wa.

[29] WSDOT. 2005. Geotechnical Design Manual M46-03, Washington State Department of Transportation, Tumwater, WA, USA.

[30] Tatsuoka, F., Hirakawa, D., Shinoda, M., Kongkitkul, W. and Uchimura, T. 2004. An old but new issue; viscous properties of polymer geosynthetic reinforcement and geosynthetic-reinforced soil structures. Keynote Lecture. In Proceedings of the 3rd Asian Regional Conference on Geosynthetics (GeoAsia 2004, editors: Shim, J. B., Yoo, C. and Jeon, H.-Y.), Seoul, Korea, pp. 29–77.

[31] Tatsuoka, F., Tateyama, M, Uchimura, T. and Koseki, J. 1997a. Geosynthetic-reinforced soil retaining walls as important permanent structures, the 1996-1997 Mercer Lecture, Geosynthetics International, 4(2), 81-136.

[32] Tatsuoka, F., Tateyama M. and Koseki, J. 1996. Performance of soil retaining walls for railway embankments, Soils and Foundations, Special Issue of Soils and Foundations on Geotechnical Aspects of the January 17 1995 HyogokenNambu Earthquake, 311-324.

[33] Tatsuoka, F. 1993. Keynote lecture: roles of facing rigidity in soil reinforcing. *In* Proceedings of the International Symposium on Earth Reinforcement Practice. Vol. 2. *Edited by* H. Ochiai, S. Hayashi, and J. Otani. A.A. Balkema, Rotterdam, The Netherlands. pp. 801–830.

[34] J.N. Mukabi, "Unique Analytical Models for Deriving Fundamental Quasi-Mechanistic Design Parameters for Highway and Airport Pavements", International Journal of Engineering Research and Technology, Volume 5, Issue 09, September 2016.

International Journal of Engineering Research & Technology (IJERT)
ISSN: 2278-0181
Vol. 7 Issue 12, December-2018

[35] Bathurst, R.J., Miyata, Y., Nernheim, A., and Allen, A.M. 2008*b*. Refinement of K-stiffness method for geosynthetic-reinforced soil walls. Geosynthetics International, **15**(4): 269–295. doi:10.1680/gein.2008.15.4.269.
[36] Rowe, R.K. and Ho, S.K. 1997. Continuous panel reinforced soil walls on rigid foundations, Journal of Geotechnical and Geoenvironmental Engineering, Vol. 123(10), pp. 912–920.
[37] Bathurst, R.J., Vlachopoulos, N., Walters, D.L., Burgess, P.G. and Allen, T.M. 2006. The influence of facing rigidity on the performance of two geosynthetic reinforced soil retaining walls, Canadian Geotechnical Journal, Vol. 43(12), pp. 1225-1237.
[38] Miyata, Y. & Bathurst, R. J. (2007a). Evaluation of K-Stiffness method for vertical geosynthetic reinforced granular soil walls in Japan. Soils and Foundations, 47, No. 2, 319–335. R.J. Bathurst and K. Hatami, "Seismic response analysis of a geosynthetic-reinforced soil retaining wall", Geosynthetics International, Vol. 5, Nos. 1-2, pp. 127-166, 1998.
[39] Ismeik, M. and Güler, E. 1998. Effect of wall facing on the seismic stability of geosynthetic-reinforced retaining walls, Geosynthetics International, 5(1&2), 41-53.
[40] Koseki, J., Bathurst, R.J., Guller, E., Kuwano, J. and Maugeri, M., "Seismic stability of reinforced soil walls", Keynote paper, 8th International Conference of Geosynthetics, Yokohama, Japan, September, 2006. 28p.
[41] Cascone, E., Maugeri, M. and Motta, E. 1995. Seismic design of earth-reinforced embankments, Earthquake Geotechnical Engineering, Balkema, 2, 1129-1134.
[42] S.M.B., Helwany, G. Reardon and J.T.H., Wu, "Effects of backfill on the performance of GRS retaining walls", Geotextiles and Geomembranes, vol. 17 (1999), pp. 1-16, 1998.
[43] Bathurst, R.J. and Hatami, K., 1998, "Seismic response analysis of a geosynthetic-reinforced soil retaining wall", Geosynthetics International, Vol. 5, Nos. 1-2, pp. 127-166.
[44] G. Moradi, "Seismic response analysis of geosynthetic reinforced soil retaining wall", EJGE, vol. 19, pp. 3819-3835, 2014.
[45] M. Khosrojerdi, M. Xiao, T. Qiu and J. Nicks, "Evaluation of prediction methods for lateral deformation of GRS walls and abutments", J. Geotech. Geoenviron. Eng., vol 143(2) 1-1, 2017.
[46] J. Xingli, X. Jinliang and S. Yuhai, "Deformation analysis of reinforced retaining wall using separate finite element", Hindawi, Discrete Dynamics in Nature and Society, vol. 2018, Article ID 6946492, 9p.